

1 Impact of Timanian thrust systems on the late 2 Neoproterozoic–Phanerozoic tectonic evolution of the 3 Barents Sea and Svalbard

4
5 Jean-Baptiste P. Koehl^{1,2,3,4}, Craig Magee⁵, Ingrid M. Anell⁶

6 ¹Centre for Earth Evolution and Dynamics (CEED), University of Oslo, PO Box 1028 Blindern, N-0315 Oslo,
7 Norway.

8 ²Department of Geosciences, UiT The Arctic University of Norway in Tromsø, N-9037 Tromsø, Norway.

9 ³Research Centre for Arctic Petroleum Exploration (ARCEX), UiT The Arctic University of Norway in Tromsø, N-
10 9037 Tromsø, Norway.

11 ⁴CAGE – Centre for Arctic Gas Hydrate, Environment and Climate, UiT The Arctic University of Norway in
12 Tromsø, N-9037 Tromsø, Norway.

13 ⁵School of Earth Science and Environment, University of Leeds, Leeds, LS2 9JT, United Kingdom.

14 ⁶Department of Geosciences, University of Oslo, P.O. Box 1047 Blindern, N-0316 Oslo, Norway.

15 **Correspondence:** Jean-Baptiste P. Koehl (jean-baptiste.koehl@uit.no)

16 17 **Abstract**

18 The Svalbard Archipelago consists of three basement terranes that record a complex
19 Neoproterozoic–Phanerozoic tectonic history, including four contractional events (Grenvillian,
20 Caledonian, Ellesmerian, and Eurekan) and two episodes of collapse- to rift-related extension
21 (Devonian–Carboniferous and late Cenozoic). Previous studies suggest these three terranes likely
22 accreted during the early–mid Paleozoic Caledonian and Ellesmerian orogenies. Yet recent
23 geochronological analyses show that the northwestern and southwestern terranes of Svalbard both
24 record an episode of amphibolite (–eclogite) facies metamorphism in the latest Neoproterozoic,
25 which may relate to the 650–550 Ma Timanian Orogeny identified in northwestern Russia, northern
26 Norway and the Russian Barents Sea. However, discrete Timanian structures have yet to be
27 identified in Svalbard and the Norwegian Barents Sea. Through analysis of seismic reflection, and
28 regional gravimetric and magnetic data, this study demonstrates the presence of continuous, several
29 kilometers thick, NNE-dipping, deeply buried thrust systems that extend thousands of kilometers
30 from northwestern Russia to northeastern Norway, the northern Norwegian Barents Sea, and the
31 Svalbard Archipelago. The consistency in orientation and geometry, and apparent linkage between

32 these thrust systems and those recognized as part of the Timanian Orogeny in northwestern Russia
33 and Novaya Zemlya suggests that the mapped structures are likely Timanian. If correct, these
34 findings would imply that Svalbard's three basement terranes and the Barents Sea were accreted
35 onto northern Norway during the Timanian Orogeny and should, hence, be attached to Baltica and
36 northwestern Russia in future Neoproterozoic–early Paleozoic plate tectonics reconstructions. In
37 the Phanerozoic, the study suggests that the interpreted Timanian thrust systems represented major
38 preexisting zones of weakness that were reactivated, folded, and overprinted by (i.e., controlled the
39 formation of new) brittle faults during later tectonic events. These faults are still active at present
40 and can be linked to folding and offset of the seafloor.

41

42 **Introduction**

43 Recognizing and linking tectonic events across different terranes is critical to plate
44 reconstructions. In the latest Neoproterozoic (at ca. 650–550 Ma), portions of northwestern Russia
45 (e.g., Timan Range and Novaya Zemlya) and the Russian Barents Sea were accreted to northern
46 Baltica by top-SSW thrusting during the Timanian Orogeny (Olovyanishnikov et al., 2000;
47 Kostyuchenko et al., 2006). Discrete Timanian structures with characteristic WNW–ESE strikes
48 are sub-orthogonal to the N–S-trending Caledonian grain formed during the closure of the Iapetus
49 Ocean (Gee et al., 1994; Witt-Nilsson et al., 1998; Johansson et al., 2004; 2005). Thus far,
50 Timanian structures have only been identified in onshore–nearshore areas of northwestern Russia
51 and northeastern Norway and offshore in the Russian Barents Sea and southeasternmost Norwegian
52 Barents Sea (Barrère et al., 2009, 2011; Marello et al., 2010; Gernigon et al., 2018; Hassaan et al.,
53 2020a, 2020b, 2021; Hassaan, 2021). Therefore, the nature of basement rocks in the northern and
54 southwestern Norwegian Barents Sea remains debatable. Some studies suggest a NE–SW-trending
55 Caledonian suture within the Barents Sea (Gudlaugsson et al., 1998; Gee and Teben'kov, 2004;
56 Breivik et al., 2005; Gee et al., 2008; Knudsen et al., 2019), whereas others argue for a swing into
57 a N–S trend and merging of Norway and Svalbard's Caledonides, which probably continue into
58 northern Greenland (Ziegler, 1988; Gernigon and Brönnner, 2012; Gernigon et al., 2014).
59 Regardless, these models solely relate basement structures in the northern and southwestern
60 Norwegian Barents Sea to the Caledonian Orogeny, implying that Laurentia and Svalbard were not
61 involved in the Timanian Orogeny and were separated from Baltica by the Iapetus Ocean in the

62 latest Neoproterozoic (Torsvik and Trench, 1991; Cawood et al., 2001; Cocks and Torsvik, 2005;
63 Torsvik et al., 2010; Merdith et al., 2021).

64 Nonetheless, geochronological data yielding Timanian ages suggest that deformation and
65 metamorphism contemporaneous of the Timanian Orogeny affected parts of the Svalbard
66 Archipelago and Laurentia and, possibly, all Arctic regions (Estrada et al., 2018; Figure 1a): (1)
67 eclogite facies metamorphism (620–540 Ma; Peucat et al., 1989; Dallmeyer et al., 1990b) and
68 eclogite facies xenoliths of mafic–intermediate granulite in Quaternary volcanic rocks are found in
69 northern Spitsbergen (648–556 Ma; Griffin et al., 2012); (2) amphibolite facies metamorphism
70 (643 ± 9 Ma; Majka et al., 2008, 2012, 2014; Mazur et al., 2009) and WNW–ESE-striking shear
71 zones like the Vimsodden–Kosibapasset Shear Zone (VKSZ; Figure 1b–c) occur in southwestern
72 Spitsbergen (600–537 Ma; Manecki et al., 1998; Faehnrich et al., 2020); and (3) xenoliths of the
73 subduction-related Midtkap igneous suite in northern Greenland yield Timanian ages (628–570
74 Ma; Rosa et al., 2016; Estrada et al., 2018). In addition, several recent studies also show the
75 presence of NW–SE- to E–W-trending basement grain in the Norwegian Barents Sea, which could
76 possibly represent Timanian fabrics and structures (Figure 1b; Barrère et al., 2009, 2011; Marello
77 et al., 2010; Klitzke et al., 2019). Following these developments, a few paleo-plate reconstructions
78 now place Svalbard together with Baltica in the latest Neoproterozoic–Paleozoic (e.g.,
79 Vernikovsky et al., 2011), and imply that the Norwegian Barents Sea and Svalbard basement may
80 contain Timanian structures overprinted during later (e.g., Caledonian) deformation events.

81 To test the origin of basement grain in the northern Norwegian Barents Sea and Svalbard,
82 the present study focuses on several kilometers deep structures identified on 2D seismic reflection
83 data and correlated using regional gravimetric and magnetic data. These newly identified structures
84 trend WNW–ESE, i.e., parallel to the Timanian structural grain in northwestern Russia and
85 northern Norway (Figure 1a–c). The structures are described and interpreted based on their
86 geometry and potential kinematic indicators, and are compared to well-known examples of
87 Caledonian and Timanian fabrics and structures elsewhere, e.g., onshore Norway (e.g., NNE-
88 dipping Trollfjorden–Komagelva Fault Zone – TKFZ; Siedlecka and Siedlecki, 1967; Siedlecka,
89 1975), in Svalbard (e.g., gently north-plunging Atomfjella Antiform – AA; Witt-Nilsson et al.,
90 1998), in northwestern Russia (NNE-dipping Central Timan Fault – CTF – and related Mikulkin
91 Antiform; Siedlecka and Roberts, 1995; Olovyanishnikov et al., 2000; Lorenz et al., 2004;
92 Kostyuchenko et al., 2006), and in the southern Norwegian Barents Sea (Barrère et al., 2011;

93 Gernigon et al., 2014) and the Russian Barents Sea (NNE-dipping Baidaratsky fault zone – BaFZ;
94 Lopatin et al., 2001; Korago et al., 2004; Figure 1b–c). The present contribution proposes a scenario
95 involving several episodes of deformation starting in the Timanian Orogeny, and involving
96 reactivation and overprinting of Timanian structures during the Caledonian Orogeny, Devonian–
97 Carboniferous extension, Triassic extension, Eurekan tectonism, and present-day tectonism.
98 Having established that Timanian structure may be present across the Barents Sea and Svalbard,
99 we briefly discuss the potential implications for the tectonic evolution of the Barents Sea and the
100 Svalbard Archipelago and associated basins (e.g., Ora and Olga basins; Anell et al., 2016).

101 Should our interpretation of discrete Timanian structures throughout the Norwegian
102 Barents Sea and Svalbard be validated by future research, it would support accretion of these
103 terranes to Baltica in the late Neoproterozoic and place the Caledonian suture farther west than is
104 commonly suggested (e.g., Breivik et al., 2005; Gernigon et al., 2014), thus leading to a major
105 revision of plate tectonics models. In addition, constraining the extent and reactivation history of
106 such faults may shed some light on their influence on younger tectonic events, such as Caledonian,
107 Ellesmerian and Eurekan contraction, Devonian–Carboniferous collapse–rifting, and late Cenozoic
108 breakup and ongoing extension.

109

110 **Geological setting**

111 *Timanian Orogeny*

112 The Timanian Orogeny corresponds to a ca. 650–550 Ma episode of NNE–SSW
113 contractional deformation that affected northwestern Russia and northeastern Norway. During this
114 tectonic episode, crustal-scale, WNW–ESE-striking, NNE-dipping thrusts systems with south-
115 southwestwards transport direction (top-SSW; Siedlecka and Siedlecki, 1967; Siedlecka, 1975;
116 Figure 1b), accreted portions of the Russian Barents Sea and northwestern Russia onto northeastern
117 Baltica, including Novaya Zemlya, Severnaya Zemlya, the Kanin Peninsula, the Timan Range, and
118 the Kola Peninsula (Siedlecka and Roberts, 1995; Olovyanishshnikov et al., 2000; Roberts and
119 Siedlecka, 2002; Gee and Pease, 2004; Kostyuchenko et al., 2006; Lorenz et al., 2008; Marelllo et
120 al., 2013) and the Varanger Peninsula in northeastern Norway (Siedlecka and Siedlecki, 1967;
121 Siedlecka, 1975; Roberts and Olovyanishshnikov, 2004; Herrevold et al., 2009; Drachev, 2016;
122 Figure 1a). Major Timanian thrusts include the NNE-dipping Baidaratsky fault zone in the Russian
123 Barents Sea and Novaya Zemlya (Figure 1a–b; Eldholm and Ewing, 1971, their figure 4 profile C–

124 D; Lopatin et al., 2001; Korago et al., 2004; Drachev, 2016), the NNE-dipping Central Timan Fault
125 (and associated thrust anticline, the Mikulkin Antiform) on the Kanin Peninsula and the Timan
126 Range (Siedlecka and Roberts, 1995; Olovyanishnikov et al., 2000; Lorenz et al., 2004;
127 Kostyuchenko et al., 2006), and the NNE-dipping Trollfjorden–Komagelva Fault Zone in northern
128 Norway (Siedlecka and Siedlecki, 1967; Siedlecka, 1975; Herrevold et al., 2009).

129

130 *Accretion of Svalbard basement terranes in the early Paleozoic*

131 The Svalbard Archipelago consists of three Precambrian basement terranes (Figure 2),
132 some of which show affinities with Greenland (northwestern and northeastern terranes), whereas
133 others are possibly derived from Pearya (southwestern terrane; Harland and Wright, 1979; Ohta et
134 al., 1989; Gee and Teben'kov, 2004; Labrousse et al., 2004; Piepjohn et al., 2013; Fortey and
135 Bruton, 2013). These terranes possibly accreted during the mid-Paleozoic Caledonian (collision of
136 Greenland with Svalbard and Norway at ca. 460–410 Ma; Horsfield, 1972; Dallmeyer et al., 1990a;
137 Johansson et al., 2004, 2005; Faehnrich et al., 2020) and Late Devonian Ellesmerian orogenies
138 (Piepjohn, 2000; Majka and Kosminska, 2017). In these models, accretion was facilitated via
139 hundreds of kilometers of displacement along (arcuate) N–S-striking strike-slip faults, such as the
140 Billefjorden Fault Zone (BFZ – Harland, 1969; Harland et al., 1992; Labrousse et al., 2008) and
141 the Lomfjorden Fault Zone (LFZ – Piepjohn et al., 2019; Figure 2), although other studies suggest
142 more limited strike-slip displacement (Lamar et al., 1986; Manby and Lyberis, 1992; Manby et al.,
143 1994; Lamar and Douglass, 1995). Some previous workers assumed that these large (strike-slip?)
144 faults extended thousands of kilometers southwards and represented the continuation of Caledonian
145 faults in Scotland (Norton et al., 1987; Dewey and Strachan, 2003). Caledonian contraction resulted
146 in the formation of large fold and thrust complexes, such as the N–S-trending, gently north-
147 plunging Atomfjella Antiform in northeastern Spitsbergen (Gee et al., 1994; Witt-Nilsson et al.,
148 1998) and the N–S-trending Rijpdalen Anticline in Nordaustlandet (Johansson et al., 2004; 2005;
149 Dumais and Brønner, 2020), whereas Ellesmerian tectonism may have formed narrow N–S-
150 trending fold and thrust belts, like the Dickson Land and Germaniahavøya fold-thrust zones
151 (McCann, 2000; Piepjohn, 2000; Dallmann and Piepjohn, 2020).

152 In northern Norway, Timanian thrusts were reactivated–overprinted in subsequent tectonic
153 events (e.g., Caledonian Orogeny and late–post-Caledonian collapse–rifting) as dominantly strike-
154 to oblique-slip faults (Siedlecka and Siedlecki, 1971; Roberts et al., 1991; Herrevold et al., 2009;

155 Rice, 2014). A notable example is the folding and reactivation of Timanian fabrics and structures
156 (e.g., NNE-dipping Trollfjorden–Komagelva Fault Zone) during the Caledonian Orogeny
157 (Siedlecka and Siedlecki, 1971; Herrevold et al., 2009) and intrusion of Mississippian dolerite
158 dykes along steeply dipping WNW–ESE-striking brittle faults that overprint the Trollfjorden–
159 Komagelva Fault Zone onshore–nearshore northern Norway (Roberts et al., 1991; Lippard and
160 Prestvik, 1997; Nasuti et al., 2015; Koehl et al., 2019).

161

162 *Late Paleozoic post-Caledonian collapse and rifting*

163 In the latest Silurian–Devonian, extensional collapse of the Caledonides led to the
164 deposition of several kilometers thick sedimentary basins such as the Devonian Graben in northern
165 Spitsbergen (Gee and Moody-Stuart, 1966; Friend et al., 1966; Friend and Moody-Stuart, 1972;
166 Murascov and Mokin, 1979; Manby and Lyberis, 1992; Manby et al., 1994; Friend et al., 1997;
167 McCann, 2000; Dallmann and Piepjohn, 2020). In places, N–S-trending basement ridges
168 potentially exhumed as metamorphic core complexes along bowed, reactivated detachments, such
169 as the Keisarhjelmen Detachment in northwestern Spitsbergen (Braathen et al., 2018).

170 In the latest Devonian–Mississippian, coal-rich sedimentary strata of the Billefjorden
171 Group were deposited within normal fault-bounded basins throughout Spitsbergen (Cutbill and
172 Challinor, 1965; Harland et al., 1974; Cutbill et al., 1976; Aakvik, 1981; Koehl and Muñoz-Barrera,
173 2018; Koehl, 2020a) and the Norwegian Barents Sea (Koehl et al., 2018a; Tonstad, 2018). As rift-
174 related normal faulting evolved, Pennsylvanian sedimentation was localized into a few, several
175 kilometers deep, N–S-trending basins like the Billefjorden Trough (Cutbill and Challinor, 1965;
176 Braathen et al., 2011; Koehl et al., 2021 in review) and the E–W-trending Ora Basin (Anell et al.,
177 2016). In the Permian, rift-related faulting stopped and platform carbonates were deposited
178 throughout Svalbard (Cutbill and Challinor, 1965) and the Barents Sea (Larssen et al., 2005).

179 Overall, the several kilometers thick, late Paleozoic sedimentary succession deposited
180 during late–post-Caledonian extension buried Proterozoic basement rocks. As a result, these rocks
181 are sparsely exposed and, thus, difficult to study.

182

183 *Mesozoic sedimentation and magmatism*

184 In the Mesozoic, Svalbard and the Barents Sea remained tectonically quiet and were only
185 affected by minor Triassic normal faulting (e.g., Anell et al., 2013; Osmundsen et al., 2014; Ogata

186 et al., 2018; Smyrak-Sikora et al., 2020). In the Early Cretaceous, Svalbard was affected by a
187 regional episode of magmatism recorded by the intrusion of numerous dykes and sills of the
188 Diabasodden Suite (Senger et al., 2013).

189

190 *Early Cenozoic Eureka tectonism*

191 The opening of the Labrador Sea and Baffin Bay between Greenland and Arctic Canada in
192 the early Cenozoic (Chalmers and Pulvercraft, 2001; Oakey and Chalmers, 2012) led to the
193 collision of northern Greenland with Svalbard and the formation of a fold-and-thrust belt with top-
194 east thrusts and east-verging folds in western Spitsbergen (Dallmann et al., 1993). In eastern
195 Spitsbergen, this deformation event is characterized by dominantly thin-skinned deformation
196 structures, including décollements, some of which showing westwards transport directions
197 (Andresen et al., 1992; Haremo and Andresen, 1992). Notably, the N–S-striking Agardhbukta
198 Fault, a major splay/segment of the N–S-striking Lomfjorden Fault Zone, accommodated reverse
199 and, possibly, strike-slip movements during this event (Piepjohn et al., 2019).

200

201 *Late Cenozoic opening of the Fram Strait*

202 After the end of extension in the Labrador Sea and Baffin Bay, the Fram Strait started to
203 open in the earliest Oligocene (Engen et al., 2008). Tectonic extension and break-up in the Fram
204 Strait resulted in the formation of two major, NW–SE-striking transform faults (Lowell, 1972;
205 Thiede et al., 1990; Figure 1b).

206

207 **Methods and datasets**

208 Seismic surveys from the DISKOS database (see Figure 1b–c and supplement S1 for
209 location) were used to interpret basement-seated structures and related, younger, brittle overprints
210 (Figure 3a–f and Figure 4a–h and supplement S2). Other features of interest include potential
211 dykes, which commonly appear as high positive reflections on seismic data. The geology
212 interpreted from onshore seismic data was directly correlated to geological maps of the Norwegian
213 Polar Institute (e.g., Dallmann, 2015). Where possible, interpretation of offshore seismic data was
214 tied to onshore geological maps and to exploration wells Raddedalen-1 and Plurdalen-1 on
215 Edgeøya (Bro and Shvarts, 1983; Harland and Kelly, 1997) and to the Hopen-2 well on Hopen
216 (Anell et al., 2014; Figure 1c and supplement S3). The Raddedalen-1 well penetrated 2823 meters

217 of Upper Permian to Mississippian or Ordovician strata, the Plurdalen well 2351 meters of Middle
218 Triassic to (pre-?) Devonian strata, and the Hopen-2 well 2840 meters of Middle–Upper Triassic
219 to Pennsylvanian strata (Bro and Shvarts, 1983; Harland and Kelly, 1997; Anell et al., 2014; Senger
220 et al., 2019). Note that the present contribution favors interpretation of lower Paleozoic
221 (Ordovician–Silurian) rocks in the Raddedalen-1 well by Bro and Shvarts (1983) to that of upper
222 Paleozoic (Upper Devonian–Mississippian) by Cambridge Svalbard Exploration (see contrasting
223 interpretations in Harland and Kelly, 1997). This is based on the more detailed lithological,
224 palynological and paleontological analyses by the former, and on the strong contrast of the
225 lithologies described in the well with Devonian–Mississippian successions on Svalbard (Cutbill
226 and Challinor, 1965; Cutbill et al., 1976; Friend et al., 1997; Dallmann and Piepjohn, 2020).

227 The present contribution only includes a few examples of seismic sections. However, more
228 interpreted and uninterpreted seismic data are available as supplements (supplements S1–2) and
229 from the Norwegian Petroleum Directorate (DISKOS database). None of the seismic sections were
230 depth-converted, and thicknesses therefore appear in seconds (Two-Way Time; TWT). However,
231 local time conversion was performed to tie seismic wells onshore Edgeøya to seismic section in
232 Storfjorden and depth conversion was performed locally to evaluate fault displacement. Velocities
233 of Gernigon et al. (2018) were used in these conversions. Supplement S3 includes further details
234 related to these conversions.

235 The boundary between Precambrian, lower Paleozoic and upper Paleozoic successions
236 offshore are interpreted as major unconformities that truncate underlying reflections and fold
237 structures (e.g., Figure 3a, b and c). The boundaries between Devonian–Permian and Mesozoic
238 successions were tied to the Raddedalen-1, Plurdalen-1, and Hopen-2 exploration wells for offshore
239 parts of the study area. The boundary between Devonian–Mississippian and Pennsylvanian–
240 Permian onshore Svalbard are interpreted as a major unconformity truncating Devonian–
241 Mississippian dykes (see Figure 3e).

242 The correlation of kilometer-thick structures discussed in the present contribution was also
243 tested using gravimetric and magnetic data in cross section (Figure 3a–f) and regional magnetic
244 and gravimetric data in the northern Norwegian Barents Sea and Svalbard (Figure 5 and supplement
245 S4) from the Federal Institute for Geosciences and Natural Resources in Germany in map view
246 (Klitzke et al., 2019). Regional gravimetric and magnetic data are also used to interpret deep
247 basement fabrics and structures, e.g., regional folds (gravimetric highs commonly associated with

248 major anticlines of thickened dense basement with high metamorphic grade (i.e., Precambrian)
249 rocks (e.g., Mikulkin Antiform; Lorenz et al., 2004; Kostyuchenko et al., 2006) and gravimetric
250 lows with synclines with less dense sedimentary basins) and large faults bounding magmatic
251 complexes and/or intruded by magmatic bodies that commonly correlate with elongated
252 gravimetric and/or magnetic anomalies (e.g., Kostyuchenko et al., 2006; Koehl et al., 2019), and
253 to discuss the relationship of the described structures with known structural trends in onshore
254 basement rocks in Russia, Norway and Svalbard. Magnetic and gravimetric anomalies not related
255 to Timanian and Caledonian grains will not be discussed in the present study.

256

257 **Results and interpretations**

258 First, the interpretation of seismic data are described by area, including (1) Storfjorden
259 (between Edgeøya and Spitsbergen) and the northeastern part of the Norwegian Barents Sea (east
260 of Edgeøya), (2) Nordmannsfonna to Sassenfjorden onshore–nearshore the eastern–central part of
261 Spitsbergen, and (3) the northwestern part of the Norwegian Barents Sea between Bjørnøya and
262 Spitsbergen (Figure 1b–c). Description in each area starts with deep Precambrian basement rocks
263 and shallow sedimentary rock units, and ends with deep brittle–ductile structures and with shallow
264 brittle faults. Then, potential field data and regional gravimetric and magnetic anomalies in the
265 Barents Sea and Svalbard are described, and compared and correlated to seismic data and to major
266 Timanian and Caledonian fabrics and structures onshore northwestern Russia, Svalbard and
267 Norway. Please see high resolution versions of all the figures and supplements on DataverseNO
268 (doi.org/10.18710/CE8RQH).

269

270 ***Structures in the northwestern–northeastern Norwegian Barents Sea, Storfjorden and central–*** 271 ***eastern Spitsbergen***

272 *Storfjorden and northeastern Norwegian Barents Sea*

273 Folded Precambrian–lower Paleozoic basement rocks

274 Seismic facies at depths of 2–6 seconds (TWT) typically comprise successions of laterally
275 discontinuous (< three kilometers long), sub-horizontal, moderately curving–undulating,
276 moderate–high-amplitude seismic reflections that alternate with packages of highly-disrupted
277 and/or curved low-amplitude seismic reflections (see yellow lines within pink and purple units in
278 Figure 3a and Figure 4a). The curving geometries of the moderate–high amplitude reflections

279 display a typical kilometer- to hundreds of meter-scale wavelength and are commonly asymmetric,
280 seemingly leaning/verging towards the south/SSW (see yellow lines in Figure 4b). Based on ties
281 with well bores on Edgeøya (Raddedalen-1 well; Bro and Shvarts, 1983; Harland and Kelly, 1997),
282 these asymmetric, undulate features most likely correspond to SSW-verging folds in Precambrian–
283 lower Paleozoic basement rocks. In places, apparent reverse offsets of these undulate reflections
284 align along moderately–gently north- to NNE-dipping surfaces (see red lines in Figure 4a and c),
285 which are therefore interpreted as minor, top-south/SSW, brittle thrusts.

286 Upper Paleozoic–Mesozoic sedimentary successions

287 In Storfjorden and the northwestern Norwegian Barents Sea, shallow (0–3 seconds TWT)
288 seismic reflections above folded and thrust Precambrian–lower Paleozoic basement rocks show
289 significantly more continuous patterns (>> five kilometers), gently curving–undulating geometries
290 and only local disruptions by shallow, dominantly NNE-dipping, high-angle listric disruptions (see
291 yellow lines within orange unit in Figure 3a and c). In the northeastern Barents Sea, these
292 reflections are largely flat-lying (see yellow lines within orange unit in Figure 3b and d). Based on
293 field mapping campaigns and well-bores in adjacent onshore areas of Spitsbergen, Edgeøya, Hopen
294 and Bjørnøya (see location in Figure 1b), these continuous reflections are interpreted as mildly
295 folded upper Paleozoic–Mesozoic (–Cenozoic?) sedimentary strata (Dallmann and Krasil'scikov,
296 1996; Harland and Kelly, 1997; Worsley et al., 2001; Dallmann, 2015). The Permian–Triassic
297 boundary was correlated throughout the northern Norwegian Barents Sea and Storfjorden by using
298 the tie of Anell et al. (2014) to the Hopen-2 well.

299 Deep thrust systems

300 The packages of sub-horizontal, moderately curving–undulating (folded Precambrian–
301 lower Paleozoic basement) reflections alternate laterally from north to south with 20–60 kilometers
302 wide, up to four seconds thick (TWT), upwards-thickening, wedge-shaped packages (areas with
303 high concentrations of black lines in Figure 3a and d). These wide upwards-thickening packages
304 consist of two types of reflections. First, they include planar, continuous, gently–moderately north-
305 to NNE-dipping, sub-parallel, high-amplitude reflections that commonly merge together
306 downwards and that can be traced and correlated on several seismic sections in Storfjorden (black
307 lines in Figure 3a). Upwards, these reflections terminate against high-amplitude convex-upwards
308 reflections interpreted as intra- Precambrian–lower Paleozoic basement reflections (fuchsia lines
309 in Figure 3a and c) or continue as moderately NNE-dipping disruption surfaces that offset these

310 intra-basement reflections top-SSW (e.g., offset intra-Precambrian unconformities in Figure 3a and
311 c and Figure 4d).

312 Second, sub-parallel, high-amplitude reflections bound wedge-shaped, upwards-thickening
313 packages of asymmetric, curved, south- to SSW-leaning, moderately north- to NNE-dipping,
314 moderate-amplitude reflections showing narrow (< one kilometer wide) upwards-convex
315 geometries (Figure 4d). These asymmetric reflections also commonly appear as gently north- to
316 NNE-dipping packages of Z-shaped reflections bounded by sub-parallel, planar, high-amplitude
317 reflections (see yellow lines in Figure 4e). Asymmetric, south- to SSW-leaning, convex-upwards
318 reflections are interpreted as south- to SSW-verging fold anticlines reflecting relatively low
319 amounts of plastic deformation of layered rocks.

320 The alternation of packages of layered rocks folded into SSW-verging folds (yellow lines
321 in Figure 3a–c) with packages of planar, NNE-dipping, sub-parallel, high-amplitude reflections
322 (black lines in Figure 3a–c) suggest that the latter reflection packages represent zones where initial
323 layering was destroyed and/or possibly reoriented, i.e., areas that accommodated larger amounts of
324 deformation and tectonic displacement. Thus, planar, gently–moderately north- to NNE-dipping,
325 high-amplitude reflections (black lines in Figure 3a–c) are interpreted as low-angle brittle–ductile
326 thrust systems. We name these thrust systems (from north to south) the Steiløya–Krylen (SKFZ),
327 Kongsfjorden–Cowanodden (KCFZ), Bellsundbanken (BeFZ), and Kinnhøgda–Daudbjørnpynten
328 fault zones (KDFZ; Figure 3a and supplement S2a–b; see Figure 1c for location of the thrusts).

329 The relatively high-amplitude character of planar, NNE-dipping reflections within the
330 thrusts suggest that these tectonic structures consist of sub-parallel layers of rocks and minerals
331 with significantly different physical properties. A probable explanation for such laterally
332 continuous and consistently high-amplitude reflections is partial recrystallization of rocks layers–
333 mineral bands into rocks and minerals with significantly higher density along intra-thrust planes
334 that accommodated large amounts of displacement (e.g., mylonitization; Fountain et al., 1984;
335 Hurich et al., 1985). In places, packages of aggregates of Z-shaped reflections bounded upwards
336 and downwards by individual low-angle thrust surfaces are interpreted as forward-dipping duplex
337 structures (e.g., Boyer and Elliott, 1982) reflecting relatively strong plastic deformation between
338 low-angle, brittle–ductile (mylonitic?) thrusts (see yellow lines in Figure 4e).

339 The Kongsfjorden–Cowanodden, Bellsundbanken, and Kinnhøgda–Daudbjørnpynten fault
340 zones can be traced east-southeast of Edgeøya as a similar series of 20–60 kilometers wide, up to

341 four seconds thick (TWT), upwards-thickening packages (e.g., black lines in Figure 3d and
342 supplements S2a). However, their imaging along NNW–SSE-trending seismic sections is much
343 more chaotic and it is more difficult to identify smaller structures (like south-verging folds and
344 minor thrusts) within each thrust system (e.g., supplement S2a). This suggests that these three thrust
345 systems strike oblique to NNW–SSE-trending seismic sections (supplement S2a), whereas they are
346 most likely sub-orthogonal to N–S- to NNE–SSW-trending seismic sections in Storfjorden (Figure
347 3a). The only orientation that reconciles these seismic facies variations (i.e., well-imaged on NNE–
348 SSW-trending seismic sections and poorly imaged by NNW–SSE-trending seismic sections;
349 Figure 3a and supplement S2a) is an overall WNW–ESE strike.

350 South of each 20–60 kilometers wide packages of thrust surfaces and related fold and
351 duplex structures, seismic reflections representing Precambrian–lower Paleozoic basement rocks
352 typically appear as gently curved, convex-upwards, relatively continuous reflections showing sub-
353 horizontal seismic onlaps (see white arrows in Figure 3a–f). This suggests that Precambrian–lower
354 Paleozoic basement rocks most likely consist (meta-) sedimentary rocks (analogous to those
355 observed in northeastern Spitsbergen and Nordaustlandet; Harland et al., 1993; Stouge et al., 2011)
356 that were deposited in foreland and piggy-back basins ahead of each 20–60 kilometers wide
357 packages (Figure 3a–f).

358 Hence, based on the upwards-thickening geometry of the packages of south- to SSW-
359 verging folds and of forward-dipping duplexes, on the top-SSW reverse offsets of intra-basement
360 reflections by low-angle brittle–ductile thrust surfaces, on the upwards truncation of these low-
361 angle thrusts by intra-basement reflections, and on the onlapping geometries of (meta-)
362 sedimentary basement rocks south of each set of top-SSW thrust surfaces, the 20–60 kilometers
363 wide, upwards-thickening, wedge-shaped packages are interpreted as crustal-scale, several
364 kilometers thick, north- to NNE-dipping, top-SSW, brittle–ductile thrust systems (see fault zones
365 with high concentration of black lines in Figure 3a–f). These thrust systems include low-angle,
366 brittle–ductile, mylonitic thrust surfaces (black lines in Figure 4d–e) separating upwards-
367 thickening thrust sheets that consist of gently to strongly folded basement rocks and forward-
368 dipping duplex structures (yellow lines in Figure 4d–e). These thrust sheets are interpreted to reflect
369 accretion and stacking from the north or north-northeast. The interpreted thrust systems are
370 comparable in seismic facies and thickness to kilometer-thick mylonitic shear zones in the

371 Norwegian North Sea (Phillips et al. 2016) and southwestern Norwegian Barents Sea (Koehl et al.,
372 2018).

373 N–S-trending folds

374 On E–W seismic cross sections, reflections of the Kongsfjorden–Cowanodden,
375 Bellsundbanken, and Kinnhøgda–Daudbjørnpynten fault zones define large, 50–100 kilometers
376 wide, U-shaped, symmetrical depressions (black lines in Figure 3b) on the edge of which they are
377 truncated at a high angle and overlain by folded lower Paleozoic and mildly folded to flat-lying
378 upper Paleozoic (meta-) sedimentary rocks (purple and orange units with associated yellow lines
379 in Figure 3b). In addition, within these U-shaped depressions, the thrust systems show curving up
380 and down, symmetrical geometries with 5–15 kilometers wavelength (yellow lines within the pink
381 unit in Figure 3b and Figure 4f). Also notice the kilometer- to hundreds of meter-scale undulating
382 pattern of 5–15 kilometers wide curved geometries (yellow lines in Figure 4f). Based on the
383 truncation and abrupt upward disappearance of high-amplitude seismic reflections characterizing
384 the thrust systems, the high-angle truncation of the thrusts is interpreted as a major erosional
385 unconformity (dark blue line in Figure 3b and pink line in Figure 4f), and the large U-shaped
386 depressions as large N–S- to NNE–SSW-trending, upright regional folds (black lines in Figure 3b).
387 Furthermore, the 5–15 kilometers wide, symmetrical, curved geometries and associated, kilometer-
388 to hundreds of meter-scale, undulating pattern of seismic reflections within the thrusts are
389 interpreted as similarly (N–S- to NNE–SSW-) trending, upright, parasitic macro- to meso-scale
390 folds (yellow lines in Figure 3b and Figure 4f).

391 Shallow brittle faults

392 In places, near the top of the 20–60 kilometers wide thrust systems (Kongsfjorden–
393 Cowanodden, Bellsundbanken, and Kinnhøgda–Daudbjørnpynten fault zones), low-angle brittle–
394 ductile thrust surfaces merge upwards with high-angle to vertical, listric, north- to NNE-dipping
395 disruption surfaces at depths of c. 2–3 seconds (TWT; see red lines in Figure 3a and d). These
396 listric disruption surfaces truncate shallow, laterally continuous reflections that display gently
397 curved, symmetric geometries in Storfjorden (yellow lines in Figure 3a) and flat-lying geometries
398 in the northeastern Norwegian Barents Sea (yellow lines in Figure 3d). Notably, they show minor,
399 down-NNE normal offsets, and related minor southwards thickening (towards the disruption) of
400 seismic sub-units within Devonian–Carboniferous (–Permian?) sedimentary strata in the north,
401 both in Storfjorden and the northeastern Barents Sea (Figure 3a–d and white double arrows in

402 Figure 4g). In addition, they display minor reverse offsets and associated gentle upright folding of
403 shallow continuous reflections potentially representing upper Mesozoic (–Cenozoic?) sedimentary
404 deposits in Storfjorden (Figure 3a–c and e, and orange lines in Figure 4h). Note that flat-lying
405 Mesozoic (–Cenozoic?) sedimentary rocks are not offset in the northeastern Norwegian Barents
406 Sea (Figure 3d).

407 Based on the observed normal offsets and southwards-thickening of Devonian–
408 Carboniferous (–Permian?) sedimentary strata north of these disruption surfaces (e.g., white double
409 arrows in Figure 4g), these are interpreted as syn-sedimentary Devonian–Carboniferous normal
410 faults. The minor reverse offsets and associated gentle upright folding of Mesozoic (–Cenozoic?)
411 sedimentary rocks in Storfjorden (e.g., orange lines in Figure 4h) suggest that these normal faults
412 were mildly inverted near Svalbard in the Cenozoic. However, it is unclear whether inversion in
413 Storfjorden initiated in the early Cenozoic or later. Nonetheless, minor reverse offset and folding
414 of the seafloor clearly indicate ongoing inversion along these faults (Figure 3a and c, and Figure
415 4h). Furthermore, considering the merging relationship between these high-angle listric disruption
416 surfaces and underlying shear zones (i.e., merging black and red lines in Figure 3a and c–d), we
417 propose that the formation of Devonian–Carboniferous normal faults was controlled by the crustal-
418 scale, north- to NNE-dipping (inherited) thrust systems (Kongsfjorden–Cowanodden,
419 Bellsundbanken, and Kinnhøgda–Daudbjørnpynten fault zones).

420

421 *Nordmannsfonna–Sassenfjorden (eastern–central Spitsbergen)*

422 Deep thrust system and N–S-trending folds

423 Seismic data from Nordmannsfonna to Sassenfjorden in eastern Spitsbergen (see Figure 1c
424 for location) show reflection packages including both planar, continuous, moderately-dipping high-
425 amplitude reflections and upwards-curving, moderate-amplitude reflections (black and yellow
426 lines in Figure 3e–f). These two sets are similar to reflection packages interpreted as low-angle,
427 brittle–ductile mylonitic thrusts bounding packages of south- to SSW-verging folds in Storfjorden
428 and the northeastern Norwegian Barents Sea (black and yellow lines in Figure 3a and d, and
429 supplement S2a). In addition, they are located at similar depths (> 2 seconds TWT) and seem to
430 align with the Kongsfjorden–Cowanodden fault zone in Storfjorden along a WNW–ESE-trending
431 axis. Hence, we interpret the deep, continuous, high-amplitude reflections in eastern Spitsbergen
432 as the western continuation of the top-SSW Kongsfjorden–Cowanodden fault zone. This thrust can

433 be traced on seismic data as gently NNE-dipping, high-amplitude reflections in Sassendalen and
434 Sassenfjorden–Tempelfjorden (supplement S2c–d), and possibly in Billefjorden (Koehl et al., 2021
435 in review, their figure 9a–b).

436 In Nordmannsfonna, the base-Pennsylvanian unconformity (white line in Figure 3e–f; tied
437 to onshore geological maps; Dallmann, 2015) truncates the Kongsfjorden–Cowanodden fault zone
438 (black lines in Figure 3e–f) upwards and the fault shows pronounced variations in dip direction,
439 ranging from east-dipping in the east to NNE-dipping in the north and WNW-dipping in the west,
440 which result into a c. 15–20 kilometers wide, north- to NNE-plunging dome-shaped/convex-
441 upwards geometry (black lines in Figure 3e–f). This portion of the thrust system is interpreted to
442 be folded into a major NNE- to north-plunging upright fold, whose 3D geometry was accurately
443 constrained due to good seismic coverage in this area (Figure 1c).

444 Small-scale structures within the Kongsfjorden–Cowanodden fault zone also show
445 asymmetric folds and internal seismic units terminating upwards with convex-upwards reflections
446 (yellow lines in Figure 3e–f) suggesting top-SSW nappe thrusting in the northern portion of the
447 thrust system. However, on E–W cross sections, seismic data reveal a set of west-verging folds in
448 the east and a more chaotic pattern of symmetrical, dominantly upright folds in the west (yellow
449 lines in Figure 3e) and below a major, high-angle, east-dipping disruption surface (thick red line in
450 Figure 3e) that crosscuts the Kongsfjorden–Cowanodden fault zone.

451 Shallow brittle faults

452 The high-angle, east-dipping disruption surface (thick red line in Figure 3e) is associated
453 with minor subvertical to steeply east-dipping disruption surfaces (thin red lines in Figure 3e). This
454 feature shows a major reverse, top-west offset (> 0.5 second TWT) of seismic units and reflections
455 at depth > 0.75 second (TWT; e.g., black lines in Figure 3e), and minor reverse offset (< 0.1 second
456 TWT) and upwards-convex curving of adjacent reflections at depth < 0.75 second (TWT; white
457 line and yellow lines within blue and units in Figure 3e). Since the major disruption coincides with
458 the location of the Agardhbukta Fault (Piepjohn et al., 2019; see Figure 1 for location) and shows
459 a steep inclination near the surface similar to that of the Agardhbukta Fault, it is interpreted as the
460 subsurface expression of this fault. The Agardhbukta Fault offsets the Kongsfjorden–Cowanodden
461 fault zone in a reverse fashion (> 0.5 second TWT; black lines in Figure 3e), and terminates upwards
462 within and slightly offsets upper Paleozoic–Mesozoic sedimentary rocks (blue and black units and
463 associated yellow lines in Figure 3e), which were correlated to onshore outcrops in eastern

464 Spitsbergen (Andresen et al., 1992; Haremo and Andresen, 1992; Dallmann, 2015). As a result,
465 these rocks are folded into a N–S-trending, open, upright fold around the fault tip, both of which
466 suggest top-west movements along the fault (Figure 3e).

467 Pre-Pennsylvanian dykes

468 In the hanging wall and on the eastern flank of the folded Kongsfjorden–Cowanodden fault
469 zone in Nordmannsfonna, high- to low-amplitude, gently east-dipping seismic reflections, which
470 possibly represent sedimentary strata (light orange unit in Figure 3e), are crosscut but not offset by
471 moderately west-dipping, high-amplitude planar reflections (blue lines in Figure 3e). In NNE–
472 SSW-trending cross-sections, these high-amplitude, cross-cutting seismic reflections appear sub-
473 horizontal (blue lines in Figure 3f). These crosscutting, west-dipping reflections are mildly folded
474 in places and either terminate upwards within the suggested, gently east-dipping, sedimentary strata
475 (light orange unit in Figure 3e) or are truncated by the base-Pennsylvanian unconformity (white
476 line in Figure 3e). Downwards within the Kongsfjorden–Cowanodden fault zone (black lines in
477 Figure 3e), these inclined reflections can be vaguely traced as a series of discontinuous, subtle
478 features (see blue lines in Figure 3e). In the footwall of the Kongsfjorden–Cowanodden fault zone,
479 the inclined reflections become more prominent again, still do not offset background reflections,
480 and extend to depths of 3–3.5 seconds (TWT; blue lines in Figure 3e). The high amplitude of these
481 planar west-dipping reflections, the absence of offset across them, and their discontinuous
482 geometries across the Agardhbukta Fault and the Kongsfjorden–Cowanodden fault zone suggest
483 that they may represent dykes (see Phillips et al., 2018). Because they appear truncated by the Base-
484 Pennsylvanian unconformity, we suggest such dykes were emplaced prior to development of this
485 unconformity. The Kongsfjorden–Cowanodden fault zone is folded into a broad, 15–20 kilometers
486 wide anticline, and offset > 0.5 second (TWT) by the Agardhbukta Fault, whereas the west-dipping
487 dykes (blue lines in Figure 3e) and the gently east-dipping sedimentary strata they intrude (light
488 orange unit in Figure 3e) are only mildly folded and show no offset across the Agardhbukta Fault
489 (Figure 3e). These differences in deformation suggest that the latter were deformed during a mild
490 episode of late contraction but not by the same early episode of intense contraction that resulted in
491 macrofolding of the Kongsfjorden–Cowanodden fault zone.

492 Cretaceous dykes and sills

493 Near or at the surface, thin, kilometer-wide, lenticular packages of gently dipping,
494 moderate–high-amplitude seismic reflections (black units in Figure 3e–f) correlate with surface

495 outcrops of Cretaceous sills of the Diabasodden Suite in eastern Spitsbergen (Senger et al., 2013;
496 Dallmann, 2015). In places, these sills are associated with areas showing high-frequency
497 disruptions of underlying sub-horizontal seismic reflections (dotted black lines in Figure 3f)
498 correlated with onshore occurrences of Pennsylvanian–Mesozoic sedimentary strata (Andresen et
499 al., 1992; Haremo and Andresen, 1992; Dallmann, 2015). We interpret these areas of high-
500 frequency disruption in otherwise relatively undisturbed and only mildly deformed Pennsylvanian–
501 Mesozoic sedimentary strata as zones with occurrences of Cretaceous feeder dykes. Alternatively,
502 disruption may be related to scattering and attenuation of seismic energy caused on the sills.

503

504 *Stappen High (northwestern Norwegian Barents Sea north of Bjørnøya)*

505 On the Stappen High between Bjørnøya and Spitsbergen (Figure 1c), seismic reflections at
506 depth of 2–6 seconds (TWT) are dominated by moderate- to high-amplitude reflections with
507 limited (< five kilometers) lateral continuity showing asymmetric, dominantly SSW-leaning
508 curving geometries with a few hundreds of meters to a few kilometers width (yellow lines within
509 pink unit in Figure 3c), i.e., analogous to those in folded Precambrian basement rocks farther north
510 (Figure 3a and Figure 4a). These reflections are truncated by gently to moderately NNE- (and
511 subsidiary SSW-) dipping disruption surfaces (black lines within pink and purple units in Figure
512 3c), some of which connect upwards with shallow (0–2 seconds TWT), NNE-dipping, high-angle
513 listric disruptions near Bjørnøya in the south (red lines in Figure 3c). Notably, major seismic
514 reflections near the upwards termination of deep, moderately–gently NNE-dipping disruption
515 surfaces display characteristic gently curving-upwards geometries (yellow lines within pink and
516 purple units in Figure 3c) and overlying seismic onlaps (white half arrows in Figure 3c) similar to
517 those observed just south of major NNE-dipping thrust systems in Storfjorden and the northeastern
518 Norwegian Barents Sea (Figure 3a and supplement S2).

519 We interpret deep (2–6 seconds TWT), curving, discontinuous seismic reflections ((yellow
520 lines within pink and purple units in Figure 3c) as folded Precambrian–lower Paleozoic basement
521 rocks, and dominantly NNE-dipping disruption surfaces (black lines within pink and purple units
522 in Figure 3) as brittle–ductile thrust possibly partly mylonitic, though with less intense deformation
523 than the major NNE-dipping thrust systems observed farther north in Storfjorden and the
524 northeastern Norwegian Barents Sea, like the Kongsfjorden–Cowanodden fault zone. These

525 brittle–ductile thrusts can be traced eastwards on seismic data on the Stappen High and into the
526 Sørkapp Basin (Figure 1c).

527 Based on their geometries and on gentle folding of the seafloor reflection (yellow lines
528 within green unit in Figure 3c), shallow, NNE-dipping, high-angle listric disruptions are interpreted
529 as mildly inverted normal faults overprinting deep NNE-dipping thrusts. Based on previous
530 fieldwork on Bjørnøya (Worsley et al., 2001), on seismic mapping in the area (Lasabuda et al.,
531 2018), and on well tie to Hopen and Edgeøya, relatively continuous (> five kilometers) shallow
532 (0–2 seconds TWT), gently curved–undulating seismic reflections overlying folded Precambrian–
533 lower Paleozoic basement rocks are interpreted as mildly folded upper Paleozoic–Mesozoic (–
534 Cenozoic?) sedimentary strata (orange and green units in Figure 3c).

535

536 ***Potential field data and regional gravimetric and magnetic anomalies***

537 *NNE-dipping thrusts*

538 In the northern Barents Sea, Storfjorden and central–eastern Spitsbergen, the seismic
539 occurrences of the Kongsfjorden–Cowanodden, Bellsundbanken and Kinnhøgda–
540 Daudbjørnpynten fault zones coincide with gradual, step-like, southwards increases in gravimetry
541 and, in places, with high magnetic anomalies in cross-section (Figure 3a–b and d–f). Similar
542 southwards gradual and step-like increases in the Bouguer and magnetic anomalies correlate with
543 major thrusts north of Bjørnøya (Figure 3c; see Figure 1b for location of Bjørnøya). These patterns
544 suggest that the footwall of the thrust systems consists of relatively denser rock units, possibly with
545 higher metamorphic grade. Seismic interpretation showing thickening of metamorphosed and
546 folded Precambrian basement rock units (pink unit in Figure 3a and c–d) in the footwall of the
547 thrusts further support this claim.

548 In map-view gravimetric and magnetic data, the three thrust systems in Storfjorden (black
549 lines in Figure 3a) coincide with three high, WNW–ESE-trending, continuous, gently undulating
550 (and, in place, merging/splaying) gravimetric and discontinuous magnetic anomalies (dashed
551 yellow lines in Figure 5a–c) that are separated from each other by areas showing relatively low
552 gravimetric and magnetic anomalies (e.g., see green to blue areas in Figure 5a). Some of these
553 anomalies extend from central Spitsbergen to Storfjorden and the northern Barents Sea (below the
554 Ora and Olga basins) as curving, E–W- and NW–SE-trending, 50–100 kilometers wide anomalies
555 (dashed yellow lines in Figure 5a–c). Analogously, thrust systems north of Bjørnøya (Figure 3c)

556 and north of the Ora and Olga basins (supplement S2b) correlate with comparable WNW–ESE-
557 trending, curving magnetic and gravimetric anomalies (dashed yellow lines in Figure 5a–c). The
558 WNW–ESE-trending anomalies appear clearer by using a slope-direction shader for gravimetric
559 data, which accentuates the contrast between each trend of anomalies (green and red areas in Figure
560 5b).

561 Most of the recognized, regional WNW–ESE-trending magnetic and gravimetric anomalies
562 (dashed yellow lines in Figure 5a–c) can be traced into the Russian Barents Sea where they are
563 linear and are crosscut by major N–S- to NNW–SSE-trending anomalies (dashed black and white
564 lines in Figure 5a–c). Subtle WNW–ESE-trending magnetic and gravimetric anomalies further
565 extend onshore northwestern Russia (e.g., Kanin Peninsula and southern Novaya Zemlya) where
566 they correlate with major Timanian thrusts and folds, some of which are suspected to extend
567 thousands of kilometers between northwestern Russia and the Varanger Peninsula in northern
568 Norway (e.g., Trollfjorden–Komagelva Fault Zone and Central Timan Fault and associated
569 Mikulkin Antiform; Siedlecka, 1975; Siedlecka and Roberts, 1995; Olovyanishnikov et al., 2000;
570 Lorenz et al., 2004; Kostyuchenko et al., 2006). In addition, two of the southernmost WNW–ESE-
571 trending gravimetric and magnetic anomalies coincide with the location of well known, crustal-
572 scale, SSW-verging Timanian thrust faults, the Trollfjorden–Komagelva Fault Zone and the
573 Central Timan Fault. Thus, based on their overall WNW–ESE trend, patterns of alternating highs
574 and lows both for gravimetric and magnetic anomalies (see Figure 5a), location at the boundary of
575 oppositely dipping slopes (see slope-direction shader map in Figure 5b), and extensive field studies
576 and seismic and well data in northwestern Russia (e.g., Kanin Peninsula and Timan Range;
577 Siedlecka and Roberts, 1995; Olovyanishnikov et al., 2000; Lorenz et al., 2004; Kostyuchenko et
578 al., 2006), northern Norway (e.g., Varanger Peninsula; Siedlecka, 1975), and the southeastern
579 Norwegian Barents Sea (Hassaan et al., 2021), WNW–ESE-trending anomalies are interpreted as
580 a combination of basement-seated Timanian macrofolds and top-SSW reverse faults (Figure 5a–
581 c).

582

583 *N–S-trending folds*

584 Large N–S-trending open folds (e.g., black and yellow lines in Figure 3b) coincide with N–
585 S- to NNE–SSW-trending, 20–100 kilometers wide, arcuate gravimetric and magnetic anomalies
586 (dashed white and black lines in Figure 5a–c), which are highly oblique to WNW–ESE-trending

587 gravimetric and magnetic anomalies and thrust systems (dashed yellow lines in Figure 5a–c).
588 Notably, major N–S- to NNE–SSW-trending synclines in Figure 3b (marked as red lines over a
589 white line in Figure 5a and c and as pink lines over a red line in Figure 5b) coincides with similarly
590 trending gravimetric and magnetic anomalies (dashed black lines in Figure 5a and c and dashed
591 white lines in Figure 5b). On the slope-direction shader map of gravimetric data, these N–S- to
592 NNE–SSW-trending anomalies are localized along the boundary between areas with eastwards-
593 (ca. 90–100°; blue areas in Figure 5b) and westwards-facing slopes (ca. 270–280°; white areas in
594 Figure 5b).

595 Notably where the main thrusts are preserved, major N–S-trending synforms (see 50–60
596 kilometers wide U-shaped depression formed by the Kinnhøgda–Daudbjørnpynten fault zone, i.e.,
597 black lines, in Figure 3b) coincide with gravimetric and magnetic highs (white and black dashed
598 lines in Figure 5a–c), whereas major antiforms where major NNE-dipping thrusts are partly eroded
599 (e.g., c. 100 kilometers wide areas where the Kinnhøgda–Daudbjørnpynten fault zone is absent in
600 Figure 3b) coincide with gravimetric and magnetic lows (the lows are parallel to white and black
601 dashed lines symbolizing magnetic and gravimetric highs in Figure 5a–c). The correlation of the
602 interpreted NNE-dipping thrust systems with gravimetric highs suggests that the thrusts consist of
603 relatively denser rocks. This supports the inferred mylonitic (i.e., higher metamorphic grade)
604 component of the thrusts because mylonites are relatively denser due to the formation of high-
605 density minerals with increasing deformation (e.g., Arbaret and Burg, 2003; Colombu et al., 2015).

606 In the northwestern part of the Barents Sea (i.e., area covered by seismic data presented in
607 Figure 3), N–S- to NNE–SSW-trending gravimetric and magnetic anomalies (white and black
608 dashed lines in Figure 5a–c) are typically 20–50 kilometers wide and correlate with similarly
609 trending Caledonian folds and thrusts onshore Nordaustlandet (e.g., Rijpdalen Anticline; Johansson
610 et al., 2004; 2005; Dumais and Brønner, 2020) and northeastern Spitsbergen (e.g., Atomfjella
611 Antiform; Gee et al., 1994; Witt-Nilsson et al., 1998), whose width is comparable to that of the
612 anomalies. In the south, N–S- to NNE–SSW-trending gravimetric and magnetic anomalies merge
613 together and swing into a NE–SW trend onshore–nearshore the Kola Peninsula and northern
614 Norway. These anomalies mimic the attitude of Caledonian thrusts and folds in the southern
615 Norwegian Barents Sea (Gernigon and Brønner, 2012; Gernigon et al., 2014) and onshore northern
616 Norway (Sturt et al., 1978; Townsend, 1987; Roberts and Williams, 2013). In the east, N–S- to

617 NNE–SSW-trending anomalies broaden to up to 150 kilometers in the Russian Barents Sea (Figure
618 5a–c).

619 In places, the intersections of high, WNW–ESE- and N–S- to NNE–SSW-trending
620 gravimetric and magnetic anomalies generate relatively higher, oval-shaped anomalies (e.g., dotted
621 white lines in Figure 5a and c). Notable examples are found in the Ora and Olga basins and east
622 and south of these basins (see dotted white lines in Figure 5a and c).

623

624 **Discussion**

625 In the discussion, we consider the lateral extent of the interpreted NNE-dipping thrust
626 systems, their possible timing of formation, and potential episodes of reactivation and overprinting.
627 Then we briefly discuss the implications of these thrust systems for plate tectonics reconstructions
628 in the Arctic.

629

630 *Extent of NNE-dipping thrust systems*

631 Four major NNE-dipping systems of mylonitic thrusts and shear zones (Steiløya–Krylen,
632 Kongsfjorden–Cowanodden, Bellsundbanken, Kinnhøgda–Daudbjørnpynten fault zones) were
633 identified at depths > 1–2 seconds (TWT) in central–eastern Spitsbergen, Storfjorden and the
634 northeastern Barents Sea, and several systems with less developed ductile fabrics between
635 Spitsbergen and Bjørnøya on the Stappen High (Figure 3a–f).

636 The Kongsfjorden–Cowanodden fault zone is relatively easy to trace and correlate in
637 Sassenfjorden, Sassendalen, Nordmannsfonna, Storfjorden and the northeastern Barents Sea (east
638 of Edgeøya) because (i) the seismic data in the these areas have a high resolution and good
639 coverage, (ii) internal seismic reflections are characterized by high amplitudes (e.g., brittle–ductile
640 thrusts and mylonitic shear zones), (iii) kinematic indicators within the thrust system consistently
641 show dominantly top–SSW sense of shear with SSW-verging fold structures (Figure 3a and d–f,
642 and supplement S2), (iv) the geometry and kinematics indicators along shallow brittle overprints
643 are regionally consistent (listric, down–NNE, brittle normal faults; Figure 3a and d–f), and (v) this
644 thrust consistently coincides with increase in gravimetric and magnetic anomaly in cross-section
645 (Figure 3a and d) and with analogously trending gravimetric and magnetic anomalies in central–
646 eastern Spitsbergen and the northern Barents Sea (Figure 5a–b). This thrust system was previously
647 identified below the Ora Basin by Klitzke et al. (2019), though interpreted as potential Timanian

648 grain instead of a discrete structure. The proposed correlation based on seismic, and cross-section
649 and map-view gravimetric and magnetic data suggests a lateral extent of c. 550–600 kilometers
650 along strike for the Kongsfjorden–Cowanodden fault zone. However, the regional magnetic and
651 gravimetric anomalies associated with this thrust in the Norwegian Barents Sea and Svalbard
652 extend potentially farther east as a series of WNW–ESE-trending anomalies to the mainland of
653 Russia (Figure 5a–c). Notably, these anomalies correlate with the southern edge of Novaya Zemlya
654 (Figure 5a–c) and, more specifically, with WNW–ESE-striking fault segments of the Baidaratsky
655 fault zone (Figure 1a; Lopatin et al., 2001; Korago et al., 2004), a major thrust fault that bounds a
656 major basement high in the central Russian Barents Sea, the Ludlov Saddle (Johansen et al., 1992;
657 Drachev et al., 2010). Thus, it is possible that the Kongsfjorden–Cowanodden fault zone also
658 extends farther east, possibly merging with the Baidaratsky fault zone, i.e., with a minimum extent
659 of 1700–1800 kilometers (Figure 5a–c). This is supported by a similar configuration of the
660 Baidaratsky Fault Zone and the Kongsfjorden–Cowanodden fault zone, including a basement-
661 seated, low-angle thrust geometry of both faults and inversion as a normal fault and deposition of
662 several seconds (TWT) thick sedimentary strata in the hanging wall of the faults in the late
663 Paleozoic (Figure 3d and Smelror et al., 2009 their profile C–D pp. 53).

664 The overall NNE-dipping and folded (into NNE-plunging folds) geometry of the
665 Kongsfjorden–Cowanodden fault zone (Figure 3e–f and Klitzke et al., 2019, their figures 3–5) may
666 explain the alternating NW–SE- and E–W-trending geometry of the gravimetric and magnetic
667 anomalies correlating with this thrust system (Figure 5a–b). E–W- and NW–SE-trending segments
668 of these anomalies may represent respectively the western and eastern limbs of open, gently NNE-
669 plunging macro-anticlines in the northern Norwegian Barents Sea. The relatively higher, oval-
670 shaped gravimetric and magnetic anomalies at the intersection of WNW–ESE- and N–S- to NNE–
671 SSW-trending magnetic and gravimetric highs, which are interpreted as the interaction of two sub-
672 orthogonal fold trends further support this claim (Figure 5a and c).

673 Interpretation of seismic sections (Figure 3e–f and supplement S2) and regional magnetic
674 and gravimetric data (Figure 5a–c) in central–eastern Spitsbergen show that NNE-dipping, top-
675 SSW Kongsfjorden–Cowanodden and Bellsundbanken fault zones likely extend westwards into
676 central (and possibly northwestern) Spitsbergen (e.g., Sassendalen, Sassenfjorden, Tempelfjorden,
677 and Billefjorden; see Figure 1c for locations). This is further supported by recent field, bathymetric
678 and seismic mapping in central Spitsbergen showing that (inverted) Devonian–Carboniferous

679 NNE-dipping brittle normal faults in Billefjorden and Sassenfjorden–Tempelfjorden merge with
680 kilometer-scale, NNE-dipping, Precambrian basement fabrics and shear zones at depth (Koehl,
681 2020a; Koehl et al., 2021 in review). Other examples of WNW–ESE-trending fabrics include faults
682 within Precambrian basement and Carboniferous sedimentary rocks in northeastern Spitsbergen
683 (Witt-Nilsson et al., 1998; Koehl and Muñoz-Barrera, 2018), and within Devonian sedimentary
684 rocks in northern and northwestern Spitsbergen (Friend et al., 1997; McCann, 2000; Dallmann and
685 Piepjohn, 2020). These suggest a repeated and regional influence of WNW–ESE-trending thrust
686 systems and associated basement fabrics in Spitsbergen.

687 Analogously to the Kongsfjorden–Cowanodden fault zone, the Bellsundbanken and
688 Kinnhøgda–Daudbjørnpynten fault zones (Figure 3a) geometries and kinematics on seismic data,
689 and their coinciding with parallel gravimetric and magnetic anomalies in map view and with
690 magnetic and gravimetric highs in cross-section suggest that they extend from Storfjorden to the
691 island of Hopen (Figure 1c, Figure 3a, Figure 5a–c, and supplement S2). Notably, a 50–100
692 kilometers wide, NNE–SSW-trending gravimetric and associated magnetic anomaly interpreted as
693 Caledonian grain in Nordaustlandet (Rijpdalen Anticline; Dumais and Brønner, 2020) bends across
694 the trace of these two thrust systems (Figure 5a–c). Farther east, the Bellsundbanken and
695 Kinnhøgda–Daudbjørnpynten fault zones parallel gravimetric and magnetic, alternating E–W- and
696 NW–SE-trending anomalies that follow the trends and map-view shapes of the Ora and Olga basins
697 in the northeastern Norwegian Barents Sea (Anell et al., 2016; see Figure 1b–c for location). This
698 suggests that these two thrust systems extend into the northeastern Norwegian Barents Sea and,
699 potentially, into the Russian Barents Sea, and affected the development of Paleozoic sedimentary
700 basins. This is also the case of the Steiløya–Krylen fault zone (supplement S2b), which coincides
701 with mild, discontinuous, WNW–ESE-trending gravimetric and magnetic anomalies that extend
702 well into the Russian Barents Sea and, possibly, across Novaya Zemlya (Figure 5a–c).

703 In southwestern Spitsbergen, field mapping revealed the presence of a major, subvertical,
704 kilometer-thick, WNW–ESE-striking mylonitic shear zone metamorphosed under amphibolite
705 facies conditions, the Vimsodden–Kosibapasset Shear Zone (Majka et al., 2008, 2012; Mazur et
706 al., 2009; see Figure 1c for location). This major sinistral shear zone aligns along a WNW–ESE-
707 trending axis with the Kinnhøgda–Daudbjørnpynten fault zone in the northwestern Norwegian
708 Barents Sea (Figure 3a), and shows a folded geometry in map view that is comparable to that of
709 major NNE-dipping thrust systems in the northern Norwegian Barents Sea (Figure 3a and e–f,

710 Figure 5a–c, and supplement S2; Klitzke et al., 2019). In addition, the Vimsodden–Kosibapasset
711 Shear Zone juxtaposes relatively old Proterozoic basement rocks in the north against relatively
712 young rocks in the south, thus suggesting a similar configuration and kinematics as along the
713 Kinnhøgda–Daudbjørnpynten fault zone in Storfjorden and the northeastern Norwegian Barents
714 Sea. Moreover, von Gosen and Piepjohn (2001) and Bergh and Grogan (2003) reported that
715 Devonian–Mississippian sedimentary successions and Cenozoic fold structures (e.g., Hyrnefjellet
716 Anticline) are offset sinistrally by a few kilometers in Hornsund. Thus, we propose that the
717 Vimsodden–Kosibapasset Shear Zone extends into Hornsund and represents the westwards
718 continuation of the Kinnhøgda–Daudbjørnpynten fault zone. This suggests a minimum extent of
719 400–450 kilometers for this thrust system (Figure 1b–c and Figure 5a–c).

720

721 ***Timing of formation of major NNE-dipping thrust systems and N–S-trending folds***

722 *NNE-dipping thrust systems*

723 The several-kilometer thickness and hundreds–thousands of kilometers along-strike extent
724 of NNE-dipping thrust systems in central–eastern Spitsbergen, Storfjorden, and the northwestern
725 and northeastern Norwegian Barents Sea suggest that they formed during a major contractional
726 tectonic event. The overall WNW–ESE trend and the consistent north-northeastwards dip and top-
727 SSW sense of shear along the newly evidenced deep thrust systems preclude formation during the
728 Grenvillian, Caledonian, and Ellesmerian orogenies, and the Eurekan tectonic event. These tectonic
729 events all involved dominantly E–W-oriented contraction and resulted in the formation of overall
730 N–S- to NNE–SSW-trending fabrics, structures and deformation belts in Svalbard (i.e., sub-
731 orthogonal to the newly identified thrust systems) such as the Atomfjella Antiform (Gee et al.,
732 1994; Witt-Nilsson et al., 1998), the Vestfonna and Rijpdalen anticlines (Johansson et al., 2004;
733 2005; Dumais and Brönnert, 2020), the Dickson Land and Germaniahelvøya fold-thrust zones
734 (McCann, 2000; Piepjohn, 2000; Dallmann and Piepjohn, 2020), and the West Spitsbergen Fold-
735 and-Thrust Belt and related early Cenozoic structures in eastern Spitsbergen (Andresen et al., 1992;
736 Haremo and Andresen, 1992; Dallmann et al., 1993), and NE–SW- to NNE–SSW-striking thrusts
737 and folds in northern Norway (Sturt et al., 1978; Townsend, 1987; Roberts and Williams, 2013)
738 and the southwestern Barents Sea (Gernigon et al., 2014).

739 A possible cause for the formation of the observed NNE-dipping thrust systems is the late
740 Neoproterozoic Timanian Orogeny, which is well known onshore northwestern Russia (e.g., Kanin

741 Peninsula, Timan Range and central Timan; Siedlecka and Roberts, 1995; Olovyanishnikov et al.,
742 2000; Lorenz et al., 2004; Kostyuchenko et al., 2006) and northeastern Norway (Varanger
743 Peninsula; Siedlecka and Siedlecki, 1967; Siedlecka, 1975; Roberts and Olovyanishnikov, 2004),
744 and traces of which were recently found in the southeastern Norwegian Barents Sea (Hassaan et
745 al., 2020a, 2020b, 2021; Hassaan, 2021), in southwestern Spitsbergen (Majka et al., 2008, 2012,
746 2014) and northern Greenland (Rosa et al., 2016; Estrada et al., 2018). The overall transport
747 direction during this orogeny was directed towards the south-southwest and most thrust systems
748 show NNE-dipping geometries (Olovyanishnikov et al., 2000; Lorenz et al., 2004; Kostyuchenko
749 et al., 2006), e.g., the Timanian thrust front on the Varanger Peninsula in northeastern Norway
750 (Trollfjorden–Komagelva Fault Zone; Siedlecka and Siedlecki, 1967; Siedlecka, 1975) and its
751 eastwards continuation, the Central Timan Fault (Lorenz et al., 2004; Kostyuchenko et al., 2006).
752 In addition, the size of Timanian thrust systems and related thrust anticlines in the Timan Range
753 and Kanin Peninsula (e.g., Central Timan Fault and Mikulkin Antiform) are comparable (≥ 3 – 4
754 seconds TWT thick thrusts and 5–15 kilometers wide thrust-related major anticlines; Lorenz et al.,
755 2004 their figures 3 and 5; Kostyuchenko et al., 2006 their figure 17) to that of thrust and fold
756 systems in the northern Norwegian Barents Sea and Svalbard (Figure 3a and c–d).

757 Thus, based on their overall WNW–ESE strike (Figure 1b–c), their vergence to the south-
758 southwest (Figure 3a, c–d and f), their coincidence with gravimetric and magnetic highs (Figure
759 5a–c), their upward truncation by a major unconformity consistently throughout the study area (see
760 top-Precambrian unconformity in Figure 3a–d), and the correlation of these NNE-dipping thrusts
761 and associated major anticlines (via gravimetric and magnetic anomalies) to similarly striking and
762 verging structures of comparable size (i.e., several seconds TWT thick, 5–15 kilometers wide
763 anticlines) onshore–nearshore northwestern Russia and northern Norway (Siedlecka, 1975;
764 Siedlecka and Roberts, 1995; Olovyanishnikov et al., 2000; Roberts and Siedlecka, 2002; Lorenz
765 et al., 2004; Gee and Pease, 2004; Kostyuchenko et al., 2006), NNE-dipping thrusts in the northern
766 Norwegian Barents Sea, Storfjorden, and central–eastern Spitsbergen are interpreted as the western
767 continuation of Timanian thrust and fold systems.

768 Timanian grain was recently identified in the northeastern Norwegian Barents Sea through
769 interpretation of new seismic, magnetic and gravimetric datasets shown in Figure 5a–c (Klitzke et
770 al., 2019). The alignment, coincident location, and matching geometries (e.g., curving E–W to
771 NW–SE strike/trend and kilometer-wide NNE–SSW-trending anticline) between Timanian grain

772 and structures mapped by Klitzke et al. (2019) and the major, NNE-dipping, top-SSW thrust
773 systems described in central–eastern Spitsbergen, Storfjorden and the Norwegian Barents Sea
774 (Figure 3a–f and supplement S2) further support a Timanian origin for the latter. Further evidence
775 of relic Timanian structural grain as far as the Loppa High and Bjørnøya Basin are documented by
776 previous magnetic studies and modelling (Marello et al., 2010). Moreover, seismic mapping
777 suggests that Timanian thrust systems extend well into central Spitsbergen (Figure 3e–f and
778 supplement S2c–d; Koehl, 2020a; Koehl et al., 2021 in review), and regional gravimetric and
779 magnetic anomaly maps suggest that Timanian thrust systems might extend farther west to (north-
780) western Spitsbergen (Figure 5a–c).

781 Probable reasons as to why these major (hundreds–thousands of kilometers long) thrust
782 systems were not identified before during fieldwork in Svalbard are their burial to high depth (>
783 1–2 seconds TWT in the study area, i.e., several kilometers below the surface; Figure 3a–f), and
784 their strong overprinting by younger tectonic events like the Caledonian Orogeny in areas where
785 they are exposed (e.g., Vimsodden–Kosibapasset Shear Zone in southwestern Spitsbergen;
786 Faehnrich et al., 2020). Possible areas of interest for future studies include the western and
787 northwestern parts of Spitsbergen where Caledonian and Eurekan E–W contraction contributed to
788 uplift and exhume deep basement rocks, and where Timanian rocks potentially crop out (e.g.,
789 Peucat et al., 1989).

790

791 *N–S-trending folds*

792 N–S-trending upright folds involve the NNE-dipping thrust systems (Figure 3b and e) and
793 correlate (via gravimetric and magnetic anomalies) with major Caledonian folds in northeastern
794 Spitsbergen and Nordaustlandet, like the Atomfjella Antiform (Gee et al., 1994; Witt-Nilsson et
795 al., 1998) and Rijpdalen Anticline (Johansson et al., 2004; 2005; Dumais and Brønner, 2020), with
796 Caledonian grain in the southern Norwegian Barents Sea (Gernigon and Brønner, 2012; Gernigon
797 et al., 2014), and with major NE–SW-trending Caledonian folds onshore northern Norway (Sturt
798 et al., 1978; Townsend, 1987; Roberts and Williams, 2013). In addition, the width of the NE–SW-
799 to N–S-trending gravimetric and magnetic anomalies associated with these folds increases up to
800 150 kilometers eastwards, i.e., away from the Caledonian collision zone (Figure 5a–c; Corfu et al.,
801 2014; Gasser, 2014). Thus, N–S-trending folds in the northern Norwegian Barents Sea are
802 interpreted as Caledonian regional folds in Precambrian–lower Paleozoic rocks. The relatively

803 broader geometry of Caledonian folds away from the Caledonian collision zone (e.g., in the
804 Russian Barents Sea) is inferred to be related to gentler fold geometries due to decreasing
805 deformation intensity in this direction. This is further supported by relatively low grade Caledonian
806 metamorphism in Franz Josef Land (Knudsen et al., 2019; see Figure 1a–b for location). By
807 contrast, the presence of tighter Caledonian folds near the collision zone in the northern Norwegian
808 Barents Sea (e.g., Figure 3b and e, and Atomfjella Antiform and Rijpdalen Anticline onshore; Gee
809 et al., 1994; Witt-Nilsson et al., 1998; Johansson et al., 2004, 2005; Dumais and Brønner, 2020) is
810 associated with much narrower (20–50 kilometers wide) gravimetric and magnetic anomalies
811 (Figure 5a–c). Note that the Atomfjella Antiform and Rijpdalen Anticline can be directly correlated
812 with 20–50 kilometers wide, N–S-trending high gravimetric and magnetic anomalies (Figure 5a–
813 c). Noteworthy, some of the NNE–SSW-trending folds and anomalies in the northernmost
814 Norwegian Barents Sea may reflect a combination of Caledonian and superimposed early Cenozoic
815 Eurekan folding (e.g., Kairanov et al., 2018).

816 The interference of WNW–ESE- and N–S- to NNE–SSW-trending gravimetric highs,
817 which are correlated to Timanian and Caledonian folds respectively, produces oval-shaped
818 gravimetric and magnetic highs (Figure 5a). These relatively higher, oval-shaped gravimetric
819 anomalies are interpreted to correspond to dome-shaped folds resulting from the interaction of
820 Timanian and Caledonian folds involving refolding of WNW–ESE-trending Timanian folds during
821 E–W Caledonian contraction. Field studies on the Varanger Peninsula in northern Norway and
822 seismic studies of Timanian thrusts off northern Norway where the interaction of Timanian and
823 Caledonian folds produced dome-shaped fold structures (Ramsay, 1962), e.g., like the Ragnarokk
824 Anticline (Siedlecka and Siedlecki, 1971; Koehl, in prep.) also support this interpretation.
825 Furthermore, Barrère et al. (2011) suggested that basins and faults in the southern Norwegian
826 Barents Sea are controlled by the interaction of Caledonian and Timanian structural grain, and
827 Marello et al. (2010) argued that elbow-shaped magnetic anomalies reflect the interaction of
828 Caledonian and Timanian structural grains in the Barents Sea, potentially as far west as the Loppa
829 High and the Bjørnøya Basin.

830

831 *Phanerozoic reactivation and overprinting of Timanian thrust systems*

832 *Caledonian reactivation and overprint*

833 The geometry of the Kongsfjorden–Cowanodden and Kinnhøgda–Daudbjørnpynten fault
834 zones in Nordmannsfonna (Figure 3e) and in the northeastern Norwegian Barents Sea (Figure 3b;
835 Klitzke et al., 2019), where they are folded into broad NNE-plunging upright anticlines and
836 synclines suggests that these thrust systems were deformed after they accommodated top-SSW
837 Timanian thrusting (Figure 6a and Figure 7a). In addition, subsidiary top-west kinematics (west-
838 verging folds and top-west minor thrusts) suggest that Timanian thrust systems were partly
839 reactivated–overprinted during an episode of intense E–W contraction (Figure 6b and Figure 7b).
840 However, west-dipping dykes crosscutting and gently east-dipping sedimentary strata overlying
841 the eastern part of the folded Kongsfjorden–Cowanodden fault zone are only mildly folded, and
842 upper Paleozoic sedimentary strata lie flat over folded and partly eroded Precambrian–lower
843 Paleozoic rocks and the Kinnhøgda–Daudbjørnpynten fault zone, thus suggesting that these
844 sedimentary strata and dykes were not involved in this episode of E–W contraction (Figure 3e).

845 A notable episode of E–W contraction in Svalbard is the Caledonian Orogeny in the early–
846 mid Paleozoic, which resulted in the formation of west-verging thrusts and N–S-trending folds of
847 comparable size (c. 15–25 kilometers wide) to those affecting the Kongsfjorden–Cowanodden and
848 Kinnhøgda–Daudbjørnpynten fault zones in Nordmannsfonna and the northern Norwegian Barents
849 Sea (Figure 3b and e; Klitzke et al., 2019, their figures 3–5), such as the Atomfjella Antiform in
850 northeastern Spitsbergen (Gee et al., 1994; Witt-Nilsson et al., 1998; Lyberis and Manby, 1999)
851 and the Rijpdalen Anticline in Nordaustlandet (Figure 1b). Since the NNE-plunging anticline in
852 Nordmannsfonna does not affect overlying Pennsylvanian–Mesozoic sedimentary strata (Figure
853 3e), we propose that they formed during Caledonian contraction (Figure 7b). This is supported by
854 the involvement of the top-Precambrian unconformity and underlying NNE-dipping thrusts in N–
855 S- to NNE-SSW-trending folds, and by the truncation of these folds by the top-Silurian
856 unconformity, which is overlapped by mildly deformed to flat-lying upper Paleozoic strata (Figure
857 3b and Figure 4f). Furthermore, structures with geometries comparable to NNE-plunging folds in
858 the northern Barents Sea and Svalbard were observed in northern Norway. An example is the
859 Ragnarokk Anticline, a dome-shaped fold structure along the Timanian front thrust on the Varanger
860 Peninsula, which results from the re-folding of Timanian thrusts and folds into a NE–SW-trending
861 Caledonian trend (Siedlecka and Siedlecki, 1971).

862 Further support of a Caledonian origin for upright NNE-plunging folds in eastern
863 Spitsbergen, Storfjorden and the northern Norwegian Barents Sea is that these folds are relatively

864 tight in the west, in Nordmannsfonna and the northwestern Barents Sea (Figure 3b and e), whereas
865 they show gradually gentler and more open geometries in the east, i.e., away from the Caledonian
866 collision zone (Figure 3b). This is also shown by the gradual eastwards broadening of regional
867 gravimetric and magnetic anomalies correlated with Caledonian folds suggesting gentler fold
868 geometries related to decreasing (Caledonian) deformation intensity in this direction (Figure 5a–c
869 and Figure 7b). This contrasts with the homogeneous intensity of deformation along NNE-dipping
870 thrusts on NNE–SSW-trending seismic profiles and with the homogeneous width of related
871 gravimetric–magnetic anomalies from west to east in Svalbard and the Barents Sea (Figure 3a–f
872 and Figure 5a–c and supplement S2). Caledonian folding of Timanian thrusts also explains the
873 weaker magnetic and gravimetric signal of Timanian faults at the location of major Caledonian
874 synclines where Timanian faults were transported downwards and, therefore, may not show well
875 on potential field data (e.g., major two, NE–SW- to N–S-trending, negative gravimetric anomalies
876 in the Russian Barents Sea just west of Novaya Zemlya; Figure 5a).

877 In Nordmannsfonna, the Caledonian origin of the major 15–20 kilometers wide anticline,
878 and the truncation of overlying, gently east-dipping, mildly folded sedimentary strata and
879 crosscutting west-dipping dykes by the base-Pennsylvanian unconformity suggest that these
880 sedimentary strata and dykes are Devonian (–Mississippian?) in age (Figure 6c–d). This is
881 supported by the presence of thick Devonian–Mississippian collapse deposits in adjacent areas of
882 central–northern Spitsbergen (Cutbill et al., 1976; Murascov and Mokin, 1979; Aakvik, 1981;
883 Gjelberg, 1983; Manby and Lyberis, 1992; Friend et al., 1997), and by Middle Devonian to
884 Mississippian ages (395–327 Ma) for dykes in central–northern Spitsbergen (Evdokimov et al.,
885 2006), northern Norway (Lippard and Prestvik, 1997; Guise and Roberts, 2002), and northwestern
886 Russia (Roberts and Onstott, 1995).

887 The occurrence of a > 0.5 second (TWT) reverse offset of the folded Kongsfjorden–
888 Cowanodden fault zone and the lack of offset of the Devonian (–Mississippian?) dykes across the
889 Agardhbukta Fault indicate that the latter fault formed as a top-west thrust during the Caledonian
890 Orogeny. At depth, the Agardhbukta Fault merges with the eastern flank of the folded
891 Kongsfjorden–Cowanodden fault zone. This, together with the presence of minor, high-angle, top-
892 west brittle thrusts within the Kongsfjorden–Cowanodden fault zone (Figure 3e), indicates that the
893 Agardhbukta Fault reactivated and/or overprinted the eastern portion of the Kongsfjorden–
894 Cowanodden fault zone in Nordmannsfonna during Caledonian contraction (Figure 6b and Figure

895 7b). Depth conversion using seismic velocities from Gernigon et al. (2018) suggest that the
896 Agardhbukta Fault offset the Kongsfjorden–Cowanodden fault zone by ca. 2.4–2.5 kilometers top-
897 west during Caledonian contraction (Figure 3e and supplement S3g). These kinematics are
898 consistent with field observation in eastern Spitsbergen by Piepjohn et al. (2019, their figure 17b).
899 However, Piepjohn et al. (2019) also suggested a significant component of Mesozoic–Cenozoic,
900 down-east normal movement, which was not identified on seismic data in Nordmannsfonna. This
901 suggests either along strike variation in the movement history of the Agardhbukta Fault, either that
902 the fault mapped on seismic data in Nordmannsfonna does not correspond to the Agardhbukta Fault
903 of Piepjohn et al. (2019).

904 Considering the presence of crustal-scale, NNE-dipping, hundreds (to thousands?) of
905 kilometers long (Timanian) thrust systems extending from the Barents Sea (and possibly from
906 onshore Russia) to central–eastern and southern Spitsbergen and the northwestern Norwegian
907 Barents Sea (Figure 5a–c) prior to the onset of E–W-oriented Caledonian contraction, it is probable
908 that such large structures would have (at least partially) been reactivated and/or overprinted during
909 subsequent tectonic events if suitably oriented. Under E–W contraction, WNW–ESE-striking,
910 dominantly NNE-dipping Timanian faults would be oriented at c. 30° to the direction of principal
911 stress and, therefore, be suitable (according to Anderson’s stress model) to reactivate/be
912 overprinted with sinistral strike-slip movements. Such kinematics were recorded along the
913 Vimsodden–Kosibapasset Shear Zone in Wedel Jarlsberg Land (Mazur et al., 2009) and within
914 Hornsund (von Gosen and Piepjohn, 2001).

915 However, recent ^{40}Ar – ^{39}Ar geochronological determinations on muscovite within this
916 structure suggest that this structure formed during the Caledonian Orogeny (Faehnrich et al. 2020).
917 Nonetheless, the same authors also obtained Timanian ages (600–540 Ma) for (initial) movements
918 along minor shear zones nearby and parallel to the Vimsodden–Kosibapasset Shear Zone. Since
919 this large shear zone must have represented a major preexisting zone of weakness when Caledonian
920 contraction initiated, it is highly probable that it was preferentially chosen to reactivate instead of
921 minor shear zones. Thus, the Caledonian ages obtained along the Vimsodden–Kosibapasset Shear
922 Zone most likely reflect complete resetting of the geochronometer along the shear zone due to large
923 amounts of Caledonian reactivation–overprinting, while minor nearby shear zones preserved traces
924 of initial Timanian deformation. This is also supported by observations in northern Norway
925 suggesting that Timanian thrusts (e.g., Trollfjorden–Komagelva Fault Zone) were reactivated as

926 major strike-slip faults during the Caledonian Orogeny (Roberts, 1972; Herrevold et al., 2009; Rice
927 2014). This interpretation reconciles the strong differences in dipping angle and depth between the
928 Kinnhøgda–Daudbjørnpynten fault zone and the Vimsodden–Kosibapasset Shear Zone. The
929 former was located away from the Caledonian collision zone and essentially retained its initial,
930 moderately NNE-dipping Timanian geometry and was deeply buried during the Phanerozoic,
931 whereas the latter was intensely deformed, pushed into a sub-vertical position, and uplifted and
932 exhumed to the surface because it was located near or within the Caledonian collision zone (Figure
933 7b).

934 This further explains why Timanian faults were not reactivated exclusively as strike-slip
935 faults despite being oriented sub-orthogonal (c. 70°) to E–W Caledonian contraction. Portions of
936 Timanian faults near the Caledonian collision zone were locally deformed into subvertical
937 geometries suitable to accommodate lateral movement, whereas their counterparts retaining their
938 moderate–low-angle dip away from the paleo-plate boundary were more prone to accommodate
939 vertical movements (Figure 7b). Moreover, lateral transport of rocks from the Caledonian collision
940 front towards the inner portions of the Barents Sea in the east was hampered by rock units
941 constituting the crust of the Barents Sea, northern Norway, northwestern Russia and other adjacent
942 areas. Hence, Caledonian E–W contraction produced more easily N–S-trending folds (e.g., Figure
943 3b and e and Figure 4f), which extended almost all the way to Novaya Zemlya (Figure 5), whereas
944 partial strike-slip reactivation was restricted to areas proximal to the Caledonian collision front
945 (e.g., western Spitsbergen; Majka et al., 2008; Mazur et al., 2009; Faehnrich et al., 2020; Ziemniak
946 et al., 2020; Figure 7b).

947

948 *Devonian–Carboniferous normal overprint–reactivation*

949 In Nordmannsfonna, the wedge shape of Devonian (–Mississippian?) sedimentary strata in
950 the hanging wall of the Kongsfjorden–Cowanodden fault zone suggest that the eastern portion of
951 this thrust was reactivated as a gently–moderately dipping extensional detachment (Figure 6c) and,
952 thus, that Devonian (–Mississippian?) strata in this area represent analogs to collapse deposits in
953 northern Spitsbergen. The intrusion of west-dipping Devonian (–Mississippian?) dykes orthogonal
954 to the eastern portion of the thrust system, i.e., orthogonal to extensional movements along the
955 inverted east-dipping portion of the thrust (Figure 3e and Figure 6d) also supports this
956 interpretation. Similar relationships were inferred in northwestern Spitsbergen, where Devonian

957 collapse sediments were deposited along a N–S-trending Precambrian basement ridge bounded by
958 a gently dipping, extensional mylonitic detachment (Braathen et al., 2018).

959 In Sassenfjorden, Storfjorden and the northeastern Norwegian Barents Sea, listric brittle
960 normal faults showing down-NNE offsets and syn-tectonic thickening within Devonian–
961 Carboniferous (–Permian?) sedimentary strata merge at depth with the uppermost part of NNE-
962 dipping Timanian thrust systems like the Kongsfjorden–Cowanodden fault zone (Figure 3a and d
963 and supplement S2c). This indicates that Timanian thrust systems were used as preexisting zones
964 of weakness during late–post-orogenic collapse of the Caledonides in the Devonian–Carboniferous
965 (Figure 6c–e and Figure 7c).

966 The presence of the Kongsfjorden–Cowanodden fault zone in Storfjorden and below
967 Edgeøya also explains the strong differences between the Paleozoic sedimentary successions
968 penetrated by the Plurdalen-1 and Raddendalen-1 exploration wells (Bro and Shvarts, 1983;
969 Harland and Kelly, 1997). Notably, the Plurdalen-1 well penetrated (at least) ca. 1600 meters thick
970 Devonian–Mississippian sedimentary rocks in the direct hanging wall of the Kongsfjorden–
971 Cowanodden fault zone and related listric brittle overprints (Figure 3a), whereas the interpretation
972 of Bro and Shvarts (1983) suggests that the Raddedalen-1 well encountered thin (90–290 meters
973 thick) Mississippian strata overlying (> 2 kilometers) thick lower Paleozoic sedimentary rocks ca.
974 30 kilometers farther northeast, i.e., away from the Kongsfjorden–Cowanodden fault zone and
975 related overprints. The presence of thick Devonian sedimentary strata in the direct hanging wall of
976 listric overprints of the Kongsfjorden–Cowanodden fault zone further supports late–post-
977 Caledonian extensional reactivation–overprinting of NNE-dipping Timanian thrusts.

978 In central Spitsbergen, recently identified Early Devonian–Mississippian normal faults
979 formed along and overprinted–reactivated major NNE-dipping ductile (mylonitic) shear zones and
980 fabrics in Billefjorden (Koehl et al., 2021 in review) and Sassenfjorden–Tempelfjorden (Koehl,
981 2020a). These show sizes, geometries and kinematics comparable to those of the Kongsfjorden–
982 Cowanodden fault zone, and are, therefore, interpreted as the western continuation of this thrust
983 system. The Devonian–Carboniferous extensional reactivation–overprinting of the Kongsfjorden–
984 Cowanodden fault zone in central Spitsbergen explains the southward provenance of northwards
985 prograding sedimentary rocks of the uppermost Silurian–Lower Devonian Siktefjellet and Red Bay
986 groups and Wood Bay Formation and the enigmatic WNW–ESE trend of the southern boundary of
987 the Devonian Graben in central–northern Spitsbergen (Gee and Moody-Stuart, 1966; Friend et al.,

988 1966; Friend and Moody-Stuart, 1972; Murascov and Mokin, 1979; Friend et al., 1997; McCann,
989 2000; Dallmann and Piepjohn, 2020; Koehl et al., 2021 in review).

990

991 *Mild Triassic overprint*

992 The Kongsfjorden–Cowanodden fault zone and associated overprints align with WNW–
993 ESE- to NW–SE-striking normal faults onshore southern and southwestern Edgeøya in
994 Kvalpynten, Negerpynten, and Øhmanfjellet (Osmundsen et al., 2014; Ogata et al., 2018). These
995 faults display both listric and steep planar geometries in cross-section and bound thickened syn-
996 sedimentary growth strata in lowermost Upper Triassic sedimentary rocks of the Tschermakfjellet
997 and De Geerdalen formations (Ogata et al., 2018; Smyrak-Sikora et al., 2020). The Norwegian
998 Barents Sea and Svalbard are believed to have remained tectonically quiet throughout the Triassic
999 apart from minor deep-rooted normal faulting in the northwestern Norwegian Barents Sea (Anell
1000 et al., 2013) and Uralides-related contraction in the (south-) east (Müller et al., 2019). Hence, we
1001 propose that the progradation and accumulation of thick sedimentary deposits of the Triassic deltaic
1002 systems above the southeastward continuation of the Kongsfjorden–Cowanodden fault zone may
1003 have triggered minor tectonic adjustments resulting in the development of a system of small half-
1004 grabens over the thrust system. Alternatively or complementary, the deposition of thick Triassic
1005 deltaic systems may have locally accelerated compaction of sedimentary strata underlying the
1006 Tschermakfjellet Formation in south- and southwest-Edgeøya, e.g., of the potential pre-Triassic
1007 syn-tectonic growth strata along the Kongsfjorden–Cowanodden fault zone, and, thus, facilitated
1008 the development of minor half-grabens within the Triassic succession along this thrust system.

1009

1010 *Eurekan reactivation–overprint*

1011 In eastern Spitsbergen, the Agardhbukta Fault segment of the Lomfjorden Fault Zone
1012 truncates the Kongsfjorden–Cowanodden fault zone with a major, > 0.5 second (TWT) top-west
1013 reverse offset (Figure 3e). The Agardhbukta fault also mildly folds Pennsylvanian–Mesozoic
1014 sedimentary rocks and Cretaceous sills into a gentle upright (fault-propagation) fold with no major
1015 offset (Figure 6f–g), which is supported by onshore field observations in eastern and northeastern
1016 Spitsbergen (Piepjohn et al., 2019). Mild folding of Mesozoic sedimentary rocks and of Cretaceous
1017 intrusions indicates that the Agardhbukta Fault was most likely mildly reactivated as a top-west
1018 thrust during the early Cenozoic Eurekan tectonic event (Figure 6g and Figure 7d).

1019 Seismic data show that high-angle listric Devonian–Carboniferous normal faults were
1020 mildly reactivated as reverse faults that propagated upwards and gently folded adjacent upper
1021 Paleozoic–Mesozoic (–Cenozoic?) sedimentary strata in the northwestern Norwegian Barents Sea,
1022 Storfjorden and central–eastern Spitsbergen (Figure 3a–c and supplement S2), but not in the
1023 northeastern Norwegian Barents Sea (Figure 3d and Figure 7d). Since normal faults were not
1024 inverted in the east, it is probable that inversion of these faults in central–eastern Spitsbergen,
1025 Storfjorden and the northwestern Norwegian Barents Sea first occurred during the Eurekan tectonic
1026 event in the early Cenozoic, when Greenland collided with western Spitsbergen (Figure 7d). This
1027 is also supported by the gently folded character of Devonian–Mesozoic (–Cenozoic?) sedimentary
1028 successions in the west (Figure 3a and c), whereas these successions are essentially flat-lying (i.e.,
1029 undeformed) in the east (Figure 3b and d). Nevertheless, folding of the seafloor reflection in
1030 Storfjorden and the northwestern Norwegian Barents Sea suggests ongoing contractional
1031 deformation along several of these faults in the northwestern Norwegian Barents Sea and
1032 Storfjorden (Figure 3a–c).

1033 Major, top-SSW mylonitic shear zones in Sassenfjorden–Tempelfjorden and Billefjorden
1034 display early Cenozoic overprints including top-SSW duplexes in uppermost Devonian–
1035 Mississippian coals of the Billefjorden Group acting as a partial décollement along a major
1036 basement-seated listric brittle fault (Koehl, 2020a; supplement S2) and NNE-dipping brittle faults
1037 offsetting the east-dipping Billefjorden Fault Zone by hundreds of meters to several kilometers left-
1038 laterally (Koehl et al., 2021 in review). Thus, the correlation of the Kongsfjorden–Cowanodden
1039 fault zone with these top-SSW mylonitic shear zones in Sassenfjorden–Tempelfjorden and
1040 Billefjorden (see Figure 1c for location) supports reactivation–overprinting of major NNE-dipping
1041 Timanian thrust systems as top-SSW, sinistral-reverse, oblique-slip thrusts in the early Cenozoic
1042 Eurekan tectonic event (Figure 7d). Such correlation explains the NW–SE trend and the location
1043 of the northeastern boundary of the Central Tertiary Basin, which terminates just southwest of
1044 Sassenfjorden and Sassendalen in central Spitsbergen (Figure 1b–c). It also explains the dominance
1045 of NW–SE- to WNW–ESE-striking faults within Cenozoic deposits of the Central Tertiary Basin
1046 (Livshits, 1965a), and the northwestwards provenance (Petersen et al., 2016) and northwards
1047 thinning of sediments deposited in the basin (Livshits, 1965b), which were probably sourced from
1048 uplifted areas in the hanging wall of the reactivated–overprinted thrust.

1049 Noteworthy, Livshits (1965a) argued that the Central Tertiary Basin was bounded to the
1050 north by a major WNW–ESE-striking fault extending from Kongsfjorden to southern Billefjorden–
1051 Sassenfjorden where the NNE-dipping Kongsfjorden–Cowanodden fault zone was mapped (present
1052 study; supplement S2). This indicates that the Kongsfjorden–Cowanodden fault zone might extend
1053 west of Billefjorden and Sassenfjorden, potentially until Kongsfjorden (see Figure 1c for location).
1054 Should it be the case, the Kongsfjorden–Cowanodden fault zone would coincide with a major
1055 terrane boundary in Svalbard, which was speculated to correspond to one or more regional WNW–
1056 ESE- to N–S-striking faults in earlier works, e.g., Kongsvegen Fault and Lapsdalen Thrust
1057 (Harland and Horsfield, 1974), Kongsvegen Fault Zone and/or Central–West Fault Zone (Harland
1058 and Wright, 1979), and Kongsfjorden–Hansbreen Fault Zone (Harland et al., 1993). The presence
1059 of a major, (inherited Timanian) NNE-dipping, basement-seated fault zone in this area would
1060 explain the observed strong differences between Precambrian basement rocks in Svalbard’s
1061 northwestern and southwestern terranes.

1062 In southern Spitsbergen, von Gosen and Piepjohn (2001) and Bergh and Grogan (2003)
1063 suggested the presence of a WNW–ESE-striking, sinistral-reverse strike-slip fault in Hornsund
1064 based on a one-kilometer left-lateral offset of Devonian–Carboniferous sedimentary successions
1065 and of the early Cenozoic Hyrnejellet Anticline across the fjord. This fault is part of the
1066 Kinnhøgda–Daudbjørnpynten fault zone and was most likely reactivated–overprinted during
1067 Eurekan contraction–transpression in the early Cenozoic.

1068

1069 *Present day tectonism*

1070 Seismic data show that the seafloor reflection is folded and/or offset in a reverse fashion by
1071 high-angle brittle faults merging at depth with interpreted Timanian thrust systems in Storfjorden
1072 and just north of Bjørnøya in the northwestern Norwegian Barents (Figure 3a and c, and Figure
1073 4h). This indicates that some of the Timanian thrust systems are still active at present and are
1074 reactivated/overprinted by reverse faults (Figure 7e). A potential explanation for ongoing
1075 reactivation–overprinting is transfer of extensional tectonic stress in the Fram Strait as ridge-push
1076 tectonism through Spitsbergen and Storfjorden (Figure 7e).

1077

1078 *Implication for plate tectonics reconstructions of the Barents Sea and Svalbard in the late*

1079 *Neoproterozoic–Paleozoic*

1080 The presence of hundreds to thousands of kilometers long Timanian faults throughout the
1081 northern Norwegian Barents Sea and central and southwestern (and possibly northwestern?)
1082 Spitsbergen indicates that the northwestern, northeastern and southwestern basement terranes of
1083 the Svalbard Archipelago were most likely already accreted together and attached to the Barents
1084 Sea, northern Norway and northwestern Russia in the late Neoproterozoic (ca. 600 Ma). Svalbard's
1085 three terranes were previously thought to have been juxtaposed during the Caledonian and
1086 Ellesmerian orogenies through hundreds–thousands of kilometers of displacement along presumed
1087 thousands of kilometers long N–S-striking strike-slip faults like the Billefjorden Fault Zone
1088 (Harland, 1969; Harland et al. 1992, Labrousse et al., 2008; Figure 2). The presence of laterally
1089 continuous (undisrupted), hundreds–thousands of kilometers long, Timanian thrust systems from
1090 southwestern and central Spitsbergen to the northern Norwegian and Russian Barents Sea clearly
1091 shows that this is not possible (Figure 8).

1092 The continuous character of these thrust systems from potentially as far as onshore
1093 northwestern Russia through the Barents Sea and Svalbard precludes any major strike-slip
1094 displacement along N–S-striking faults such as the Billefjorden Fault Zone and Lomfjorden Fault
1095 Zone (as proposed by Harland et al., 1974, 1992; Labrousse et al., 2008; Figure 2) and any hard-
1096 linked connection between these faults in Svalbard and analogous, NE–SW-striking faults in
1097 Scotland in the Phanerozoic (as proposed by Harland, 1969). Instead, the present work suggests
1098 that the crust constituting the Barents Sea and the northeastern and southwestern basement terranes
1099 of Svalbard should be included as part of Baltica in future Arctic plate tectonics reconstructions for
1100 the late Neoproterozoic–Paleozoic period (i.e., until ca. 600 Ma; Figure 8). It also suggests that the
1101 Caledonian suture zone, previously inferred to lie east of Svalbard in the Barents Sea (e.g., Gee
1102 and Teben'kov, 2004; Breivik et al., 2005; Barrère et al., 2011; Knudsen et al., 2019) may be
1103 located west of the presently described Timanian thrust systems, i.e., probably west of or in western
1104 Spitsbergen where Caledonian blueschist and eclogite metamorphism has been recorded in
1105 Precambrian basement rocks (Horsfield, 1972; Dallmeyer et al., 1990a; Ohta et al., 1995;
1106 Kosminska et al., 2014).

1107

1108 **Conclusions**

1109 1) Seismic data in the northern Norwegian Barents Sea and Svalbard reveal the existence of
1110 several systems of hundreds–thousands of kilometers long, several kilometers thick, top-

1111 SSW thrusts comprised of brittle–ductile thrusts, mylonitic shear zones and associated
1112 SSW-verging folds that appear to extend from onshore northwestern Russia to the northern
1113 Norwegian Barents Sea and to central and southwestern Spitsbergen. A notable structure is
1114 the Kongsfjorden–Cowanodden fault zone in Svalbard and the Norwegian Barents Sea,
1115 which likely merges with the Baidaratsky fault zone in the Russian Barents Sea and
1116 southern Novaya Zemlya. We interpret these thrust systems as being related to the
1117 Neoproterozoic Timanian Orogeny.

1118 2) In the east (away from the Caledonian collision zone), these Timanian thrusts systems were
1119 folded into NNE-plunging folds, offset, and reactivated as and/or overprinted by top-west,
1120 oblique-slip sinistral-reverse, brittle–ductile thrusts during subsequent Caledonian (e.g.,
1121 Agardhbukta Fault segment of the Lomfjorden Fault Zone) and, possibly, during Eurekan
1122 contraction, and are deeply buried. By contrast, in the west (near or within the Caledonian
1123 collision zone), Timanian thrusts were intensely deformed, pushed into sub-vertical
1124 positions, extensively overprinted, and exhumed to the surface.

1125 3) In eastern Spitsbergen, a major NNE-dipping Timanian thrust system, the Kongsfjorden–
1126 Cowanodden fault zone, is crosscut by a swarm of Devonian (–Mississippian?) dykes that
1127 intruded contemporaneous sedimentary strata deposited during extensional reactivation of
1128 the eastern portion of the thrust system as a low-angle extensional detachment during late–
1129 post-Caledonian collapse.

1130 4) Timanian thrust systems were overprinted by NNE-dipping, brittle normal faults in the late
1131 Paleozoic during the collapse of the Caledonides and/or subsequent rifting in the Devonian–
1132 Carboniferous.

1133 5) Timanian thrust systems and associated Caledonian and Devonian–Carboniferous brittle
1134 overprints (e.g., Agardhbukta Fault) in the northwestern Norwegian Barents Sea and
1135 Svalbard were mildly reactivated during the early Cenozoic Eurekan tectonic event, which
1136 resulted in minor folding and minor reverse offsets of Devonian–Mesozoic sedimentary
1137 strata and intrusions. Timanian thrusts and related overprints in the northeastern Norwegian
1138 Barents Sea were not reactivated during the Eurekan tectonic event.

1139 6) The presence of hundreds–thousands of kilometers long Timanian thrust systems may
1140 suggest that the Barents Sea and Svalbard’s three basement terranes were already attached
1141 to northern Norway and northwestern Russia in the late Neoproterozoic (ca. 600 Ma). If

1142 correct, a Timanian origin for these structures would preclude any major strike-slip
1143 movements along major N–S-striking faults like the Billefjorden and Lomfjorden fault
1144 zones in the Phanerozoic, and imply that the Caledonian suture zone is located west of or
1145 in western Spitsbergen.

1146

1147 **Acknowledgements**

1148 The present study was supported by the Research Council of Norway, the Tromsø Research
1149 Foundation, and six industry partners through the Research Centre for Arctic Petroleum
1150 Exploration (ARCEX; grant number 228107), the SEAMSTRESS project (grant number 287865),
1151 and the Centre for Earth Evolution and Dynamics (CEED; grant number 223272). We thank the
1152 Norwegian Petroleum Directorate and the Federal Institute for Geosciences and Natural Resources
1153 (BGR) for granting access and allowing publication of seismic, magnetic and gravimetric data in
1154 Svalbard and the Norwegian Barents Sea. Prof. Steffen Bergh, Dr. Winfried Dallmann, Prof. Jiri
1155 Konopasek, Assoc. Prof. Mélanie Forien, Dr. Kate Waghorn (UiT The Arctic University of Norway
1156 in Tromsø), Dr. Peter Klitzke (Federal Institute for Geosciences and Natural Resources –
1157 Germany), Anna Dichiarante (Norway Seismic Array), Rune Mattingdal (Norwegian Petroleum
1158 Directorate), and Prof. Carmen Gaina (Centre for Earth Evolution and Dynamics, University of
1159 Oslo) are thanked for fruitful discussion.

1160

1161 **Data availability**

1162 For high-resolution versions of the figures and supplements, the reader is referred to the
1163 Open Access data repository DataverseNO (doi.org/10.18710/CE8RQH).

1164

1165 **References**

- 1166 Aakvik, R.: Fasies analyse av Undre Karbonske kullførende sedimenter, Billefjorden, Spitsbergen,
1167 Ph.D. Thesis, University of Bergen, Bergen, Norway, 219 pp., 1981.
- 1168 Andresen, A., Haremo, P., Swensson, E. and Bergh, S. G.: Structural geology around the southern
1169 termination of the Lomfjorden Fault Complex, Agardhdalen, east Spitsbergen, Norsk Geol.
1170 Tidsskr., 72, 83–91, 1992.
- 1171 Anell, I., Braathen, A., Olaussen, S. and Osmundsen, P. T.: Evidence of faulting contradicts a
1172 quiescent northern Barents Shelf during the Triassic, First Break, 31, 67–76, 2013.

- 1173 Anell, I. M., Braathen, A. and Olaussen, S.: Regional constraints of the Sørkapp Basin: A
1174 Carboniferous relic or a Cretaceous depression, *Mar. Petrol. Geol.*, 54, 123–138, 2014.
- 1175 Anell, I. M., Faleide, J. I. and Braathen, A.: Regional tectono-sedimentary development of the
1176 highs and basins of the northwestern Barents Shelf, *Norsk Geologisk Tidsskrift*, 96, 1, 27–
1177 41, 2016.
- 1178 Arbaret, L. and Burg, J.-P.: Complex flow in lowest crustal, anastomosing mylonites: Strain
1179 gradients in a Kohistan gabbro, northern Pakistan, *J. Geophys. Res.*, 108, 2467, 2003.
- 1180 Barrère, C., Ebbing, J. and Gernigon, L.: Offshore prolongation of Caledonian structures and
1181 basement characterization in the western Barents Sea from geophysical modelling,
1182 *Tectonophys.*, 470, 71–88, 2009.
- 1183 Barrère, C., Ebbing, J. and Gernigon, L.: 3-D density and magnetic crustal characterization of the
1184 southwestern Barents Shelf: implications for the offshore prolongation of the Norwegian
1185 Caledonides, *Geophys. J. Int.*, 184, 1147–1166, 2011.
- 1186 Boyer, S. E. and Elliott, D.: Thrust Systems, *AAPG Bulletin*, 66, 9, 1196–1230, 1982.
- 1187 Braathen, A., Bælum, K., Maher Jr., H. D. and Buckley, S. J.: Growth of extensional faults and
1188 folds during deposition of an evaporite-dominated half-graben basin; the Carboniferous
1189 Billefjorden Trough, Svalbard, *Norsk Geol. Tidsskr.*, 91, 137–160, 2011.
- 1190 Braathen, A., Osmundsen, P. T., Maher, H. and Ganerød, M.: The Keisarhjelmen detachment
1191 records Silurian–Devonian extensional collapse in Northern Svalbard, *Terra Nova*, 30, 34–
1192 39, 2018.
- 1193 Breivik, A. J., Mjelde, R., Grogan, P., Shimamura, H., Murai, Y. and Nishimura, Y.: Caledonide
1194 development offshore–onshore Svalbard based on ocean bottom seismometer, conventional
1195 seismic, and potential field data, *Tectonophys.*, 401, 79–117, 2005.
- 1196 Bro, E. G. and Shvarts, V. H.: Processing results from drill hole Raddedalen-1, Edge Island,
1197 Spitzbergen Archipelago, All-Russian Research Institute for Geology and Mineral
1198 Resources of the World Ocean, St. Petersburg, *Pangaea*, Report 5750, 1983.
- 1199 Cawood, P. A., McCausland, P. J. A. and Dunning, G. R.: Opening Iapetus: Constraints from the
1200 Laurentian margin in Newfoundland, *GSA Bull.*, 113, 4, 443–453, 2001.
- 1201 Chalmers, J. A. and Pulvertaft, T. C. R.: Development of the continental margins of the Labrador
1202 Sea: a review, in: *Non-Volcanic Rifting of Continental Margins: A Comparison of*

- 1203 Evidence from Land and Sea, edited by: Wilson, R. C. L., Taylor, R. B. and Froitzheim,
1204 N., Geol. Soc. London, Spec. Publi., 187, 77–105, 2001.
- 1205 Cocks, L. R. M. and Torsvik, T. H.: Baltica from the late Precambrian to mid-Palaeozoic times:
1206 The gain and loss of a terrane's identity, *Earth-Sci. Rev.*, 72, 39–66, 2005.
- 1207 Colombu, S., Cruciani, G., Fancello, D., Franceschelli, M. and Musumeci, G.: Petrophysical
1208 properties of a granite-protomylonite-ultramylonite sequence: insight from the Monte
1209 Grighini shear zone, central Sardinia, Italy, *Eur. J. Mineral*, 27, 471–486, 2015.
- 1210 Corfu, F., Andersen, T. B. and Gasser, D.: The Scandinavian Caledonides: main features,
1211 conceptual advances and critical questions, in: *New Perspectives on the Caledonides of*
1212 *Scandinavia and Related Areas*, edited by: Corfu, F., Gasser, D. and Chew, D. M., Geol.
1213 Soc., London, Spec. Publi., 390, 9–43, 2014.
- 1214 Cutbill, J. L. and Challinor, A.: Revision of the Stratigraphical Scheme for the Carboniferous and
1215 Permian of Spitsbergen and Bjørnøya, *Geol. Mag.*, 102, 418–439, 1965.
- 1216 Cutbill, J. L., Henderson, W. G. and Wright, N. J. R.: The Billefjorden Group (Early Carboniferous)
1217 of central Spitsbergen, *Norsk Polarinst. Skr.*, 164, 57–89, 1976.
- 1218 Dallmann, W. K.: *Geoscience Atlas of Svalbard*, Norsk Polarinstitutt, Tromsø, Norway,
1219 Rapportserie nr. 148, 2015.
- 1220 Dallmann, W. K. and Krasil'scikov, A. A.: Geological map of Svalbard 1:50,000, sheet D20G
1221 Bjørnøya, *Norsk Polarinst. Temakart*, 27, 1996.
- 1222 Dallmann, W. K. and Piepjohn, K.: The structure of the Old Red Sandstone and the Svalbardian
1223 Orogenic Event (Ellesmerian Orogeny) in Svalbard, *Norg. Geol. Unders. B., Spec. Publi.*,
1224 15, 106 pp., 2020.
- 1225 Dallmeyer, R. D., Peucat, J. J., Hirajima, T. and Ohta, Y.: Tectonothermal chronology within a
1226 blueschist–eclogite complex, west-central Spitsbergen, Svalbard: Evidence from $^{40}\text{Ar}/^{39}\text{Ar}$
1227 and Rb–Sr mineral ages, *Lithos*, 24, 291–304, 1990a.
- 1228 Dallmeyer, R. D., Peucat, J. J. and Ohta, Y.: Tectonothermal evolution of contrasting metamorphic
1229 complexes in northwest Spitsbergen (Biskayerhalvøya): Evidence from $^{40}\text{Ar}/^{39}\text{Ar}$ and Rb-
1230 Sr mineral ages, *GSA Bull.*, 102, 653–663, 1990b.
- 1231 Dewey, J. F. and Strachan, R. A.: Changing Silurian–Devonian relative plate motion in the
1232 Caledonides: sinistral transpression to sinistral transtension, *J. Geol. Soc., London*, 160,
1233 219–229, 2003.

- 1234 Drachev, S. S.: Fold belts and sedimentary basins of the Eurasian Arctic, *Arktos*, 2:21, 2016.
- 1235 Drachev, S. S., Malyshev, N. A. and Nikishin, A. M.: Tectonic history and petroleum geology of
1236 the Russian Arctic Shelves: an overview, *Petrol. Geol. Conf. series*, 7, 591–619, 2010.
- 1237 Dumais, M.-A. and Brønner, M.: Revisiting Austfonna, Svalbard, with potential field methods – a
1238 new characterization of the bed topography and its physical properties, *The Cryosphere*,
1239 14, 183–197, 2020.
- 1240 Eldholm, O. and Ewing, J.: Marine Geophysical Survey in the Southwestern Barents Sea, *J.*
1241 *Geophys. Res.*, 76, 17, 3832–3841, 1971.
- 1242 Engen, Ø., Faleide, J. I. and Dyreng, T. K.: Opening of the Fram Strait gateway: A review of plate
1243 tectonic constraints, *Tectonophys.*, 450, 51–69, 2008.
- 1244 Estrada, S., Tessensohn, F. and Sonntag, B.-L.: A Timanian island-arc fragment in North
1245 Greenland: The Midtkap igneous suite, *J. Geodyn.*, 118, 140–153, 2018.
- 1246 Faehnrich, K., Majka, J., Schneider, D., Mazur, S., Manecki, M., Ziemniak, G., Wala, V. T. and
1247 Strauss, J. V.: Geochronological constraints on Caledonian strike-slip displacement in
1248 Svalbard, with implications for the evolution of the Arctic, *Terra Nova*, 2020, 32, 290–299.
- 1249 Fortey, R. A. and Bruton, D. L.: Lower Ordovician trilobites of the Kirtonryggen Formation,
1250 Spitsbergen, *ossils and Strata*, 59, Wiley Blackwell, 120 pp., 2013.
- 1251 Fountain, D. M., Hurich, C. A. and Smithson, S. B.: Seismic relectivity of mylonite zones in the
1252 crust, *Geology*, 12, 195–198, 1984.
- 1253 Friend, P. F. and Moody-Stuart, M.: Sedimentation of the Wood Bay Formation (Devonian) of
1254 Spitsbergen: Regional analysis of a late orogenic basin, *Norsk Polarinst. Skr.*, 157, 80 pp.,
1255 1972.
- 1256 Friend, P. F., Heintz, N. and Moody-Stuart, M.: New unit terms for the Devonian of Spitsbergen
1257 and a new stratigraphical scheme for the Wood Bay Formation, *Polarinst. Årbok*, 1965, 59–
1258 64, 1966.
- 1259 Friend, P. F., Harland, W. B., Rogers, D. A., Snape, I. and Thornley, R. S.: Late Silurian and Early
1260 Devonian stratigraphy and probable strike-slip tectonics in northwestern Spitsbergen, *Geol.*
1261 *Mag.*, 134, 4, 459–479, 1997.
- 1262 Gasser, D.: The Caledonides of Greenland, Svalbard and other Arctic areas: status of research and
1263 open questions, in: *New Perspectives on the Caledonides of Scandinavia and Related Areas*,

- 1264 edited by: Corfu, F., Gasser, D. and Chew, D. M., Geol. Soc., London, Spec. Publi., 390,
1265 93–129, 2014.
- 1266 Gee, D. G. and Moody-Stuart, M.: The base of the Old Red Sandstone in central north Haakon VII
1267 Land, Vestspitsbergen, Polarinst. Årbok, 1964, 57–68, 1966.
- 1268 Gee, D. G. and Pease, V.: The Neoproterozoic Timanide Orogen of eastern Baltica: introduction,
1269 in: The Neoproterozoic Timanide Orogen of eastern Baltica, edited by: Gee, D. G. and
1270 Pease, V., Geol. Soc. London, Mem., 30, 1–3, 2004.
- 1271 Gee, D. G. and Teben'kov, A. M.: Svalbard: a fragment of the Laurentian margin, in: The
1272 Neoproterozoic Timanide Orogen of eastern Baltica, edited by: Gee, D. G. and Pease, V.,
1273 Geol. Soc. London, Mem., 30, 191–206, 2004.
- 1274 Gee, D. G., Björklund, L. and Stølen, L.-K.: Early Proterozoic basement in Ny Friesland–
1275 implications for the Caledonian tectonics of Svalbard, Tectonophys., 231, 171–182, 1994.
- 1276 Gee, D. G., Fossen, H., Henriksen, N. and Higgins, A. K.: From the Early Paleozoic Platforms of
1277 Baltica and Laurentia to the Caledonide Orogen of Scandinavia and Greenland, Episodes,
1278 31, 1, 44–51, 2008.
- 1279 Gernigon, L. and Brönnner, M.: Late Palaeozoic architecture and evolution of the southwestern
1280 Barents Sea: insights from a new generation of aeromagnetic data, J. Geol. Soc., London,
1281 169, 449–459, 2012.
- 1282 Gernigon, L., Brönnner, M., Roberts, D., Olesen, O., Nasuti, A. and Yamasaki, T.: Crustal and basin
1283 evolution of the southwestern Barents Sea: From Caledonian orogeny to continental
1284 breakup, Tectonics, 33, 347–373, 2014.
- 1285 Gernigon, L., Brönnner, M., Dumais, M.-A., Gradmann, S., Grønlie, A., Nasuti, A. and Roberts, D.:
1286 Basement inheritance and salt structures in the SE Barents Sea: Insights from new potential
1287 field data, J. Geodyn., 119, 82–106, 2018.
- 1288 Griffin, W. L., Nikolic, N., O'Reilly, S. Y. and Pearson, N. J.: Coupling, decoupling and
1289 metasomatism: Evolution of crust–mantle relationships beneath NW Spitsbergen, Lithos,
1290 149, 115–135, 2012.
- 1291 Gudlaugsson, S. T., Faleide, J. I., Johansen, S. E. and Breivik, A. J.: Late Palaeozoic structural
1292 development of the South-western Barents Sea. Mar. Petrol. Geol., 15, 73–102, 1998.
- 1293 Haremo, P. and Andresen, A.: Tertiary décollements thrusting and inversion structures along
1294 Billefjorden and Lomfjorden Fault Zones, East Central Spitsbergen, in: Structural and

- 1295 Tectonic Modelling and its Application to Petroleum Geology, edited by: Larsen, R. M.,
 1296 Brekke, H., Larsen, B. T. and Talleraas, E., Norwegian Petroleum Society (NPF) Special
 1297 Publications, 1, 481–494, 1992.
- 1298 Harland, W. B.: Contribution of Spitsbergen to understanding of tectonic evolution of North
 1299 Atlantic region, AAPG Memoirs, 12, 817–851, 1969.
- 1300 Harland, W. B. and Horsfield, W. T.: West Spitsbergen Orogen, in: Mesozoic–Cenozoic Orogenic
 1301 Belts, data for Orogenic Studies, J. Geol. Soc. London, Spec. Publi., 4, 747–755, 1974.
- 1302 Harland, W. B. and Kelly, S. R. A.: Eastern Svalbard Platform, in: Geology of Svalbard, edited by:
 1303 Harland, W. B., Geol. Soc. London, Mem., 17, 521 pp., 1997.
- 1304 Harland, W. B. and Wright, N. J. R.: Alternative hypothesis for the pre-Carboniferous evolution of
 1305 Svalbard, Norsk Polarinst. Skr., 167, 89–117, 1979.
- 1306 Harland, W. B., Cutbill, L. J., Friend, P. F., Gobbett, D. J., Holliday, D. W., Maton, P. I., Parker,
 1307 J. R. and Wallis, R. H.: The Billefjorden Fault Zone, Spitsbergen – the long history of a
 1308 major tectonic lineament, Norsk Polarinst. Skr., 161, 1–72, 1974.
- 1309 Harland, W. B., Scott, R. A., Auckland, K. A. and Snape, I.: The Ny Friesland Orogen, Spitsbergen,
 1310 Geol. Mag., 129, 6, 679–708, 1992.
- 1311 Harland, W. B., Hambrey, M. J. and Waddams, P.: Vendian geology of Svalbard, Norsk Polarinst.
 1312 Skri., 193, 152 pp., 1993.
- 1313 Hassaan, M.: Evaporite-influenced rift basins and salt tectonics in the southeastern Norwegian
 1314 Barents Sea, Ph.D. Thesis, University of Oslo, Oslo, Norway, 305 pp., 2021.
- 1315 Hassaan, M., Faleide, J. I., Gabrielsen, R. H. and Tsikalas, F.: Carboniferous graben structures,
 1316 evaporite accumulations and tectonic inversion in the southeastern Norwegian Barents Sea,
 1317 Mar. Petrol. Geol., 112, 104038, 2020a.
- 1318 Hassaan, M., Faleide, J. I., Gabrielsen, R. H. and Tsikalas, F.: Architecture of the evaporite
 1319 accumulation and salt structures dynamics in Tiddlybanken Basin, southeastern Norwegian
 1320 Barents Sea, Basin Res., 33, 91–117, 2020b.
- 1321 Hassaan, M., Faleide, J. I., Gabrielsen, R. H. and Tsikalas, F.: Effects of basement structures and
 1322 Carboniferous basin configuration on evaporite distribution and the development of salt
 1323 structures in Nordkapp Basin, Barents Sea—Part I, Basin Res., 33, 4, 2474–2499, 2021.

- 1324 Herrevold, T., Gabrielsen, R. H. and Roberts, D.: Structural geology of the southeastern part of the
1325 Trollfjorden-Komagelva Fault Zone, Varanger Peninsula, Finnmark, North Norway,
1326 Norwegian Journal of Geology, 89, 305-325, 2009.
- 1327 Horsfield, W. T.: Glauconite schists of Caledonian age from Spitsbergen, Geol. Mag., 109, 1,
1328 29–36, 1972.
- 1329 Hurich, C. A., Smithson, S. B., Fountain, D. M. and Humphreys, M. C.: Seismic evidence of
1330 mylonite reflectivity and deep structure in the Kettle dome metamorphic core complex,
1331 Washington, Geology, 13, 577–580, 1985.
- 1332 Jakobsson, M., Mayer, L., Coackley, B., Dowdeswell, J. A., Forbes, S., Fridman, B., Hodnesdal,
1333 H., Noormets, R., Pedersen, R., Rebesco, M., Schenke, H. W., Zarayskaya, Y., Accettella,
1334 D., Armstrong, A., Anderson, R. M., Bienhoff, P., Camerlenghi, A., Church, I., Edwards,
1335 M., Gardner, J. V., Hall, J. K., Hell, B., Hestvik, O., Kristoffersen, Y., Marcussen, C.,
1336 Mohammad, R., Mosher, D., Nghiem, S. V., Pedrosa, M. T., Travaglini, P. G., and
1337 Weatherall, P.: The International Bathymetric Chart of the Arctic Ocean (IBCAO) Version
1338 3.0, Geophys. Res. Lett., 39, L12609, <https://doi.org/10.1029/2012GL052219>, 2012.
- 1339 Johansen, S. E., Ostistiy, B. K., Birkeland, Ø., Fedorovsky, Y. F., Martirosjan, V. N., Bruun
1340 Christensen, O., Cheredeev, S. I., Ignatenko, E. A. and Margulis, L. S.: Hydrocarbon
1341 potential in the Barents Sea region: play distribution and potential, in: Arctic Geology and
1342 Petroleum Potential, edited by: Vorren, T. O., Bergsager, E., Dahl-Stammes, Ø. A., Holter,
1343 E., Johansen, B., Lie, E. and Lund, T. B., NPF Spec. Publi., 2, 273–320, Elsevier,
1344 Amsterdam, 1992.
- 1345 Johansson, Å., Larionov, A. N., Gee, D. G., Ohta, Y., Tebenkov, A. M. and Sandelin, S.:
1346 Grenvillian and Caledonian tectono-magmatic activity in northeasternmost Svalbard, in:
1347 The Neoproterozoic Timanide Orogen of Eastern Baltica, edited by: Gee, D. G. and Pease,
1348 V., Geol. Soc. London Memoirs, 30, 207–232, 2004.
- 1349 Johansson, Å., Gee, D. G., Larionov, A. N., Ohta, Y. and Tebenkov, A. M.: Grenvillian and
1350 Caledonian evolution of eastern Svalbard – a tale of two orogenies, Terra Nova, 17, 317–
1351 325, 2005.
- 1352 Kairanov, B., Escalona, A., Mordascova, A., Sliwiska, K. and Suslova, A.: Early Cretaceous
1353 tectonostratigraphy evolution of the north central Barents Sea, J. Geodyn., 119, 183–198,
1354 2018.

- 1355 Klitzke, P., Franke, D., Ehrhardt, A., Lutz, R., Reinhardt, L., Heyde, I. and Faleide, J. I.: The
1356 Palaeozoic Evolution of the Olga Basin Region, Northern Barents Sea: A Link to the
1357 Timanian Orogeny, *Geochem., Geophys., Geosy.*, 20, 614–629, 2019.
- 1358 Knudsen, C., Gee, D. G., Sherlock, S. C. and Yu, L.: Caledonian metamorphism of metasediments
1359 from Franz Josef Land, *GFF*, 141, 295–307, 2019.
- 1360 Koehl, J.-B. P.: Early Cenozoic Eureka strain partitioning and decoupling in central Spitsbergen,
1361 Svalbard, *Solid Earth*, 12, 1025–1049, 2020a.
- 1362 Koehl, J.-B. P.: Impact of Timanian thrusts on the Phanerozoic tectonic history of Svalbard,
1363 Keynote lecture, EGU General Assembly, May 3rd–8th 2020, Vienna, Austria, 2020b.
- 1364 Koehl, J.-B. P. and Muñoz-Barrera, J. M.: From widespread Mississippian to localized
1365 Pennsylvanian extension in central Spitsbergen, Svalbard, *Solid Earth*, 9, 1535–1558, 2018.
- 1366 Koehl, J.-B. P., Bergh, S. G., Henningsen, T. and Faleide, J. I.: Middle to Late Devonian–
1367 Carboniferous collapse basins on the Finnmark Platform and in the southwesternmost
1368 Nordkapp basin, SW Barents Sea, *Solid Earth*, 9, 341–372, 2018.
- 1369 Koehl, J.-B. P., Bergh, S. G., Osmundsen, P. T., Redfield, T., Indrevær, K., Lea, H. and Bergø, E.:
1370 Late Devonian–Carboniferous faulting and controlling structures and fabrics in NW
1371 Finnmark, *Norw. J. Geol.*, 99, 3, 1–40, 2019.
- 1372 Koehl, J.-B. P., Allaart, L. and Noormets, R.: Devonian–Carboniferous collapse and segmentation
1373 of the Billefjorden Trough, and Eureka inversion–overprint and strain partitioning and
1374 decoupling along inherited WNW–ESE-striking faults, in review, 2021.
- 1375 Korago, E. A., Kovaleva, G. N., Lopatin, B. G. and Orgo, V. V.: The Precambrian rocks of Novaya
1376 Zemlya, in: *The Neoproterozoic Timanide Orogen of Eastern Baltica*, edited by: Gee, D.
1377 G. and Pease, V., *Geol. Soc. London, Mem.*, 30, 135–143, 2004.
- 1378 Kosminska, K., Majka, J., Mazur, S., Krumbholz, M., Klonowska, I., Manecki, M., Czerny, J. and
1379 Dwornik, M.: Blueschist facies metamorphism in Nordenskiöld Land of west-central
1380 Svalbard, *Terra Nova*, 26, 377–386, 2014.
- 1381 Kostyuchenko, A., Sapozhnikov, R., Egorkin, A., Gee, D. G., Berzin, R. and Solodilov, L.: Crustal
1382 structure and tectonic model of northeastern Baltica, based on deep seismic and potential
1383 field data, in: *European Lithosphere Dynamics*, edited by: Gee, D. G. and Stephenson, R.
1384 A., *Geol. Soc. London Mem.*, 32, 521–539, 2006.

- 1385 Labrousse, L., Elvevold, S., Lepvrier, C. and Agard, P.: Structural analysis of high-pressure
1386 metamorphic rocks of Svalbard: Reconstructing the early stages of the Caledonian orogeny,
1387 *Tectonics*, 27, 22 pp., 2008.
- 1388 Lamar, D. L. and Douglass, D. N.: Geology of an area astride the Billefjorden Fault Zone, Northern
1389 Dicksonland, Spitsbergen, Svalbard, *Polarist. Skr.*, 197, 46 pp., 1995.
- 1390 Lamar, D. L., Reed, W. E. and Douglass, D. N.: Billefjorden fault zone, Spitsbergen: Is it part of a
1391 major Late Devonian transform?, *GSA*, 97, 1083–1088, 1986.
- 1392 Larssen, G. B., Elvebakk, G., Henriksen, L. B., Kristensen, S.-E., Nilsson, I., Samuelsberg, T. J.,
1393 Svånå, T. A., Stemmerik, L. and Worsley, D.: Upper Palaeozoic lithostratigraphy of the
1394 Southern part of the Norwegian Barents Sea, *Norges geol. unders. Bull.*, 444, 45 pp., 2005.
- 1395 Lasabuda, A., Laberg, J. S., Knutsen, S.-M. and Safronova, P.: Cenozoic tectonostratigraphy and
1396 pre-glacial erosion: A mass-balance study of the northwestern Barents Sea margin,
1397 Norwegian Arctic, *J. Geodyn.*, 119, 149–166, 2018.
- 1398 Lippard, S. J. and Prestvik, T.: Carboniferous dolerite dykes on Magerøy: new age determination
1399 and tectonic significance, *Norsk Geologisk Tidsskrift*, 77, 159-163, 1997.
- 1400 Livshits, Yu. Ya.: Tectonics of Central Vestspitsbergen, in: *Geology of Spitsbergen*, edited by:
1401 Sokolov, V. N., National Lending Library of Science and Technology, Boston Spa.,
1402 Yorkshire, UK, 59–75, 1965a.
- 1403 Livshits, Yu. Ya.: Paleogene deposits of Nordenskiöld Land, Vestspitsbergen, in: *Geology of*
1404 *Spitsbergen*, edited by: Sokolov, V. N., National Lending Library of Science and
1405 Technology, Boston Spa., Yorkshire, UK, 193–215, 1965b.
- 1406 Lopatin, B. G., Pavlov, L. G., Orgo, V. V. and Shkarubo, S. I.: Tectonic Structure of Novaya
1407 Zemlya, *Polarforschung*, 69, 131–135, 2001.
- 1408 Lorenz, H., Pystin, A. M., Olovyanishnikov, V. G. and Gee, D. G.: Neoproterozoic high-grade
1409 metamorphism of the Kanin Peninsula, Timanide Orogen, northern Russia, in: *The*
1410 *Neoproterozoic Timanide Orogen of Eastern Baltica*, edited by: Gee, D. G. and Pease, V.,
1411 *Geol. Soc. London, Mem.*, 30, 59–68, 2004.
- 1412 Lorenz, H., Männik, P., Gee, D. and Proskurnin, V.: Geology of the Severnaya Zemlya Archipelao
1413 and the North Kara Terrane in the Russian high Arctic, *Int. J. Earth Sci.*, 97, 519–547, 2008.
- 1414 Lowell, J. D.: Spitsbergen tertiary Orogenic Belt and the Spitsbergen Fracture Zone, *GSA Bull.*,
1415 83, 3091–3102, 1972.

- 1416 Lyberis, N. and Manby, G.: Continental collision and lateral escape deformation in the lower and
1417 upper crust: An example from Caledonide Svalbard, *Tectonics*, 18, 1, 40–63, 1999.
- 1418 Majka, J. and Kosminska, K.: Magmatic and metamorphic events recorded within the Southwestern
1419 Basement Province of Svalbard, *Arktos*, 3:5, 2017.
- 1420 Majka, J., Mazur, S., Manecki, M., Czerny, J. and Holm, D. K.: Late Neoproterozoic amphibolite-
1421 facies metamorphism of a pre-Caledonian basement block in southwest Wedel Jarlsberg
1422 Land, Spitsbergen: new evidence from U–Th–Pb dating of monazite, *Geol. Mag.*, 145, 6,
1423 822–830, 2008.
- 1424 Majka, J., Larionov, A. N., Gee, D. G., Czerny, J. and Prsek, J.: Neoproterozoic pegmatite from
1425 Skoddefjellet, Wedel Jarlsberg Land, Spitsbergen: Additional evidence for c. 640 Ma
1426 tectonothermal event in the Caledonides of Svalbard, *Polish Polar Res.*, 33, 1–17, 2012.
- 1427 Majka, J., De’eri-Shlevin, Y., Gee, D. G., Czerny, J., Frei, D. and Ladenberger, A.: Torellian (c.
1428 640 Ma) metamorphic overprint of Tonian (c. 950 Ma) basement in the Caledonides of
1429 southwestern Svalbard, *Geol. Mag.*, 151, 4, 732–748, 2014.
- 1430 Manby, G. M. and Lyberis, N.: Tectonic evolution of the Devonian Basin of northern Spitsbergen,
1431 *Norsk Geol. Tidsskr.*, 72, 7–19, 1992.
- 1432 Manby, G. M., Lyberis, N., Chorowicz, J. and Thiedig, F.: Post-Caledonian tectonics along the
1433 Billefjorden fault zone, Svalbard, and implications for the Arctic region, *Geol. Soc. Am.
1434 Bul.*, 105, 201–216, 1994.
- 1435 Manecki, M., Holm, D. K., Czerny, J. and Lux, D.: Thermochronological evidence for late
1436 Proterozoic (Vendian) cooling in southwest Wedel Jarlsberg Land, Spitsbergen, *Geological
1437 Magazine*, 135, 63–9, 1998.
- 1438 Marello, L., Ebbing, J. and Gernigon, L.: Magnetic basement study in the Barents Sea from
1439 inversion and forward modelling, *Tectonophys.*, 493, 153–171, 2010.
- 1440 Marello, L., Ebbing, J. and Gernigon, L.: Basement inhomogeneities and crustal setting in the
1441 Barents Sea from a combined 3D gravity and magnetic model, *Geophys. J. Int.*, 193, 2,
1442 557–584, 2013.
- 1443 Mazur, S., Czerny, J., Majka, J., Manecki, M., Holm, D., Smyrak, A. and Wypych, A.: A strike-
1444 slip terrane boundary in Wedel Jarlsberg Land, Svalbard, and its bearing on correlations of
1445 SW Spitsbergen with the Pearya terrane and Timanide belt, *J. Geol. Soc. London*, 166, 529–
1446 544, 2009.

- 1447 McCann, A. J.: Deformation of the Old Red Sandstone of NW Spitsbergen; links to the Ellesmerian
1448 and Caledonian orogenies, in: *New Perspectives on the Old Red Sandstone*, edited by:
1449 Friends, P. F. and Williams, B. P. J., Geol. Soc. London, 180, 567–584, 2000.
- 1450 Merdith, A. S., Williams, S. E., Collins, A. S., Tetley, M. G., Mulder, J. A., Blades, M. L., Young,
1451 A., Armistead, S. E., Cannon, J., Zahirovic, S. and Müller, R. D.: Extending full-plate
1452 tectonic models into deep time: Linking the Neoproterozoic and the Phanerozoic, *Earth-*
1453 *Sci. Rev.*, 214, 103477, 2021.
- 1454 Müller, R., Klausen, T. G., Faleide, J. I., Olaussen, S., Eide, C. H. and Suslova, A.: Linking regional
1455 unconformities in the Barents Sea to compression-induced forebulge uplift at the Triassic-
1456 Jurassic transition, *Tectonophys.*, 765, 35–51, 2019.
- 1457 Murascov, L. G. and Mokin, Ju. I.: Stratigraphic subdivision of the Devonian deposits of
1458 Spitsbergen, *Polarinst. Skr.*, 167, 249–261, 1979.
- 1459 Nasuti, A., Roberts, D. and Gernigon, L.: Multiphase mafic dykes in the Caledonides of northern
1460 Finnmark revealed by a new high-resolution aeromagnetic dataset, *Norwegian Journal of*
1461 *Geology*, 95, 251-263, 2015.
- 1462 Norton, M. G., McClay, K. R. and Way, N. A.: Tectonic evolution of Devonian basins in northern
1463 Scotland and southern Norway, *Norsk Geol. Tidsskr.*, 67, 323–338, 1987.
- 1464 Oakey, G. N. and Chalmers, J. A.: A new model for the Paleogene motion of Greenland relative to
1465 North America: Plate reconstructions of the Davis Strait and Nares Strait regions between
1466 Canada and Greenland, *J. of Geophys. Res.*, 117, B10401, 2012.
- 1467 Ogata, K., Mulrooney, M. J., Braathen, A., Maher, H., Osmundsen, P. T., Anell, I., Smyrak-Sikora,
1468 A. A. and Balsamo, F.: Architecture, deformation style and petrophysical properties of
1469 growth fault systems: the Late Triassic deltaic succession of southern Edgeøya (East
1470 Svalbard), *Basin Res.*, 30, 5, 1042–1073, 2018.
- 1471 Ohta, Y., Dallmeyer, R. D. and Peucat, J. J.: Caledonian terranes in Svalbard, *GSA Spec. Paper*,
1472 230, 1–15, 1989.
- 1473 Ohta, Y., Krasil'scikov, A. A., Lepvrier, C. and Teben'kov, A. M.: Northern continuation of
1474 Caledonian high-pressure metamorphic rocks in central-western Spitsbergen, *Polar Res.*,
1475 14, 3, 303–315, 1995.

- 1476 Olovyanishshnikov, V. G., Roberts, D. and Siedlecka, A.: Tectonics and Sedimentation of the
1477 Meso- to Neoproterozoic Timan-Varanger Belt along the Northeastern Margin of Baltica,
1478 *Polarforschung*, 68, 267–274, 2000.
- 1479 Osmundsen, P-T., Braathen, A., Rød, R. S. and Hynne, I. B.: Styles of normal faulting and fault-
1480 controlled sedimentation in the Triassic deposits of Eastern Svalbard, Norwegian Petroleum
1481 directorate Bulletin, 10, 61–79, 2014.
- 1482 Petersen, T. G., Thomsen, T. B., Olausen, S. and Stemmerik, L.: Provenance shifts in an evolving
1483 Eureka foreland basin: the Tertiary Central Basin, Spitsbergen, *J. Geol. Soc., London*, 173,
1484 634–648, 2016.
- 1485 Peucat, J.-J., Ohta, Y., Gee, D. G. and Bernard-Griffiths, J.: U-Pb, Sr and Nd evidence for
1486 Grenvillian and latest Proterozoic tectonothermal activity in the Spitsbergen Caledonides,
1487 *Arctic Ocean, Lithos*, 22, 275–285, 1989.
- 1488 Phillips, T., Jackson, C. A-L., Bell, R. E., Duffy, O. B. and Fossen, H.: Reactivation of
1489 intrabasement structures during rifting: A case study from offshore southern Norway,
1490 *Journal of Structural Geology*, 91, 54–73, 2016.
- 1491 Piepjohn, K.: The Svalbardian–Ellesmerian deformation of the Old Red Sandstone and the pre-
1492 Devonian basement in NW Spitsbergen (Svalbard), in: *New Perspectives on the Old Red*
1493 *Sandstone*, edited by: Friend, P. F. and Williams, B. P. J., *Geol. Soc. London Spec. Publi.*,
1494 180, 585–601, 2000.
- 1495 Piepjohn, K.: von Gosen, W., Läufer, A., McClelland, W. C. and Estrada, S.: Ellesmerian and
1496 Eureka fault tectonics at the northern margin of Ellesmere Island (Canadian High Arctic),
1497 *Z. Dt. Ges. Geowiss.*, 164, 1, 81–105, 2013.
- 1498 Piepjohn, K., Dallmann, W. K. and Elvevold, S.: The Lomfjorden Fault Zone in eastern Spitsbergen
1499 (Svalbard), in: *Circum-Arctic Structural Events: Tectonic Evolution of the Arctic Margins*
1500 *and Trans-Arctic Links with Adjacent Orogens*, edited by: Piepjohn, K., Strauss, J. V.,
1501 Reinhardt, L. and McClelland, W. C., *GSA Spec. Paper*, 541, 95–130, 2019.
- 1502 Ramsay, J. G.: Interference Patterns Produced by the Superposition of Folds of Similar Type, *J.*
1503 *Geol.*, 70, 4, 466–481, 1962.
- 1504 Rice, A. H. N.: Restoration of the External Caledonides, Finnmark, North Norway, in: *New*
1505 *Perspectives on the Caledonides of Scandinavia and Related Areas*, Corfu, F., Gasser, D.

1506 and Chew, D. M. (eds), Geological Society, London, Special Publications, 390, 271-299,
1507 2014.

1508 Roberts, D.: Tectonic Deformation in the Barents Sea Region of Varanger Peninsula, Finnmark,
1509 Norges geol. unders., 282, 1–39, 1972.

1510 Roberts, D. and Olovyanishshnikov, V.: Structural and tectonic development of the Timanide
1511 orogeny, in: The Neoproterozoic Timanide Orogen of Eastern Baltica, edited by: Gee, D.
1512 G. and Pease, V., Geol. Soc. London, Mem., 30, 47–57, 2004.

1513 Roberts, D. and Siedlecka, A.: Timanian orogenic deformation along the northeastern margin of
1514 Baltica, Northwest Russia and Northeast Norway, and Avalonian-Cadomian connections,
1515 Tectonophysics, 352, 169-184, 2002.

1516 Roberts, D. and Williams, G. D.: Berggrunnskart Kjøllefjord 2236 IV, M 1:50.000, foreløpig
1517 utgave, Norges geol. unders., 2013.

1518 Roberts, D., Mitchell, J. G. and Andersen, T. B.: A post-Caledonian dyke from Magerøy North
1519 Norway: age and geochemistry, Norwegian Journal of Geology, 71, 289-294, 1991.

1520 Rosa, D., Majka, J., Thrane, K. and Guarnieri, P.: Evidence for Timanian-age basement rocks in
1521 North Greenland as documented through U–Pb zircon dating of igneous xenoliths from the
1522 Midtkap volcanic centers, Precambrian Res., 275, 394–405, 2016.

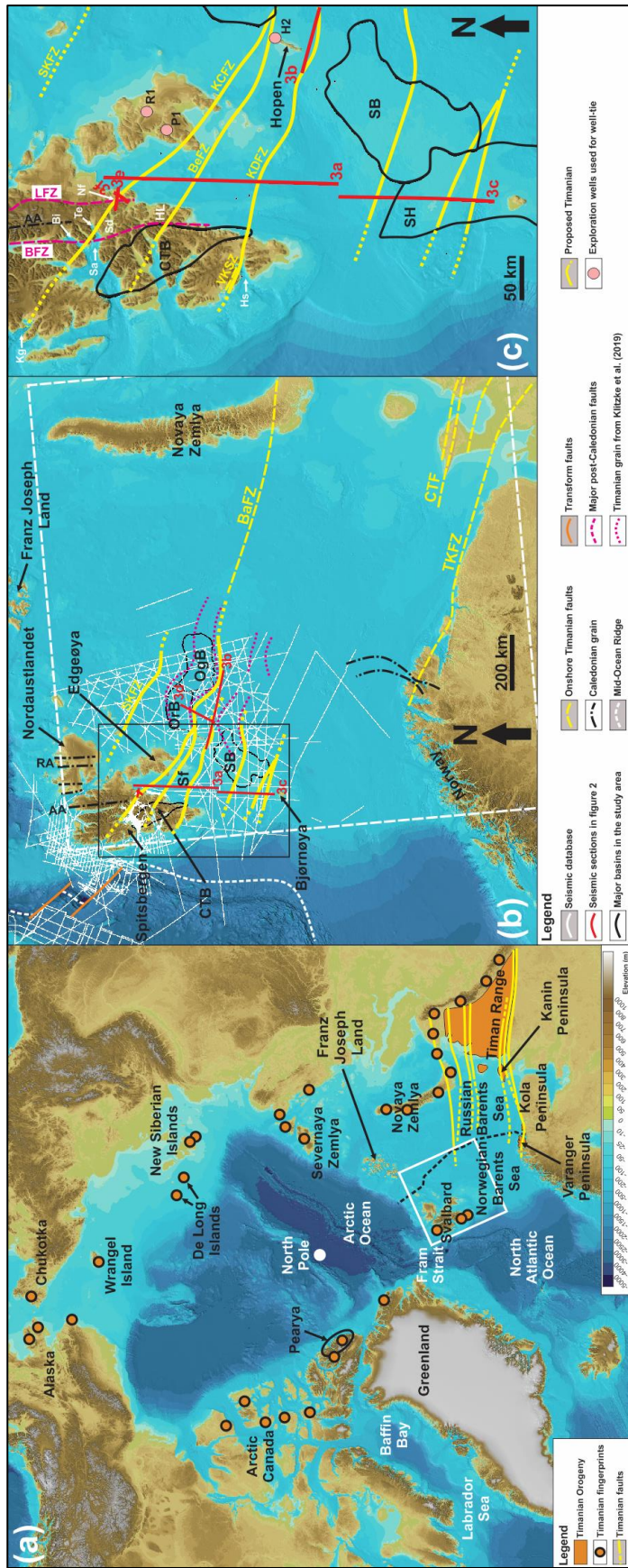
1523 Schiffer, C., Doré, A. G., Foulger, G. R., Franke, D., Geoffroy, L., Gernigon, L., Holdsworth, B.,
1524 Kuszniir, N., Lundin, E., McCaffrey, K., Peace, A. L., Petersen, K. D., Phillips, T. B.,
1525 Stephenson, R., Stoker, M. S. and Welford, J. K.: Structural inheritance in the North
1526 Atlantic, Earth-Science Reviews, 206, 102975, 2020.

1527 Senger, K., Roy, S., Braathen, A., Buckley, S., Bælum, K., Gernigon, L., Mjelde, R., Noormets,
1528 R., Ogata, K., Olausson, S., Planke, S., Ruud, B. O. and Tveranger, J.: Geometries of
1529 doleritic intrusions in central Spitsbergen, Svalbard: an integrated study of an onshore-
1530 offshore magmatic province with applications to CO₂ sequestration, Norw. J. Geol., 93,
1531 143–166, 2013.

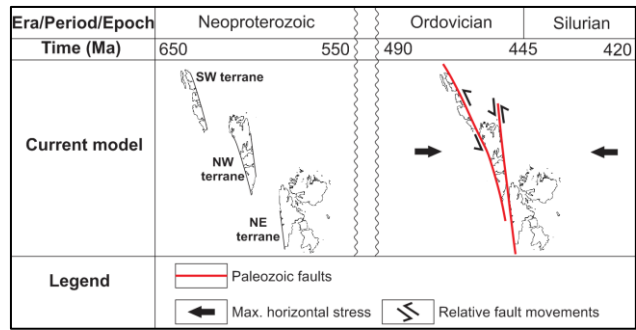
1532 Siedlecka, A.: Late Precambrian Stratigraphy and Structure of the North-Eastern Margin of the
1533 Fennoscandian Shield (East Finnmark – Timan Region), Nor. geol. unders., 316, 313-348,
1534 1975.

- 1535 Siedlecka, A. and Roberts, D.: Report from a visit to the Komi Branch of the Russian Academy of
1536 Sciences in Syktyvkar, Russia, and from fieldwork in the central Timans, August 1995,
1537 Norges geol. unders. report, 95.149, 32 pp., 1995.
- 1538 Siedlecka, A. and Siedlecki, S.: Some new aspects of the geology of Varanger peninsula (Northern
1539 Norway), *Nor. geol. unders.*, 247, 288-306, 1967.
- 1540 Siedlecka, A. and Siedlecki, S.: Late Precambrian sedimentary rocks of the Tanafjord–
1541 Varangerfjord region of Varanger Peninsula, Northern Norway, in: *The Caledonian
1542 Geology of Northern Norway*, edited by: Roberts, D. and Gustavson, M., *Norges geol.
1543 unders.*, 269, 246–294, 1971.
- 1544 Smelror, M., Petrov, O. V., Larssen, G. B. and Werner, S. C.: *Geological Atlas of the Barents Sea*,
1545 Geological Survey of Norway, Trondheim, Norway, 2009.
- 1546 Smyrak-Sikora, A., Osmundsen, P. T., Braathen, A., Ogata, K., Anell, I., Mulrooney, M. J. and
1547 Zuchuat, V.: Architecture of growth basins in a tidally influenced, prodelta to delta-front
1548 setting: The Triassic succession of Kvalpynten, East Svalbard, *Basin Research*, 32, 5, 959–
1549 988, 2020.
- 1550 Stouge, S., Christiansen, J. L. and Holmer, L. E.: Lower Palaeozoic stratigraphy of
1551 Murchisonfjorden and Sparreneset, Nordaustlandet, Svalbard, *Geografiska Annaler: Series
1552 A, Physical Geography*, 93, 209–226, 2011.
- 1553 Sturt, B. A., Pringle, I. R. and Ramsay, D. M.: The Finnmarkian phase of the Caledonian Orogeny,
1554 *J. Geol., Soc., London*, 135, 597–610, 1978.
- 1555 Thiede, J., Pfirman, S., Schenke, H.-W. and Reil, W.: Bathymetry of Molloy Deep: Fram Strait
1556 Between Svalbard and Greenland, *Mar. Geophys. Res.*, 12, 197–214, 1990.
- 1557 Tonstad, S. A.: The Late Paleozoic development of the Ottar basin from seismic 3D interpretation,
1558 Master's Thesis, University of Tromsø, Tromsø, Norway, 135 pp., 2018.
- 1559 Torsvik, T. H. and Trench, A.: The Ordovician history of the Iapetus Ocean in Britain: new
1560 palaeomagnetic constraints, *J. Geol. Soc., London*, 148, 423–425, 1991.
- 1561 Torsvik, T. H., Burke, K., Steinberger, B., Webb, S. J. and Ashwal, L. D.: Diamond sampled by
1562 plumes from the core–mantle boundary, *Nature Lett.*, 466, 352–355, 2010.
- 1563 Townsend, C.: Thrust transport directions and thrust sheet restoration in the Caledonides of
1564 Finnmark, North Norway, *J. Structural Geol.*, 9, 3, 345–352, 1987.

- 1565 Vernikovsky, V. A., Metelkin, D. V., Vernikovskaya, A. E., Matushkin, N. Yu., Lobkovsky, L. I.
1566 and Shipilov, E. V.: Early evolution stage of the arctic margins (Neoproterozoic-Paleozoic)
1567 and plate reconstructions, ICAM VI Proceedings, May 2011, Fairbanks, Alaska, USA, 265–
1568 285, 2011.
- 1569 Von Gosen, W. and Piepjohn, K.: Polyphase Deformation in the Eastern Hornsund Area, *Geol. Jb.*,
1570 B91, 291–312, 2001.
- 1571 Witt-Nilsson, P., Gee, D. G. and Hellman, F. J.: Tectonostratigraphy of the Caledonian Atomfjella
1572 Antiform of northern Ny Friesland, Svalbard, *Norsk Geol. Tidsskr.*, 78, 67–80, 1998.
- 1573 Worsley, D., Agdestein, T., Gjelberg, J. G., Kirkemo, K., Mørk, A., Nilsson, I., Olausen, S., Steel,
1574 R. J. and Stemmerik, L.: The geological evolution of Bjørnøya, Arctic Norway:
1575 implications for the Barents Shelf, *Norsk Geol. Tidsskr.*, 81, 195–234, 2001.
- 1576 Ziegler, P. A.: Evolution of the Arctic–North Atlantic and the Western Tethys, *AAPG Mem.* 43,
1577 1988.
- 1578

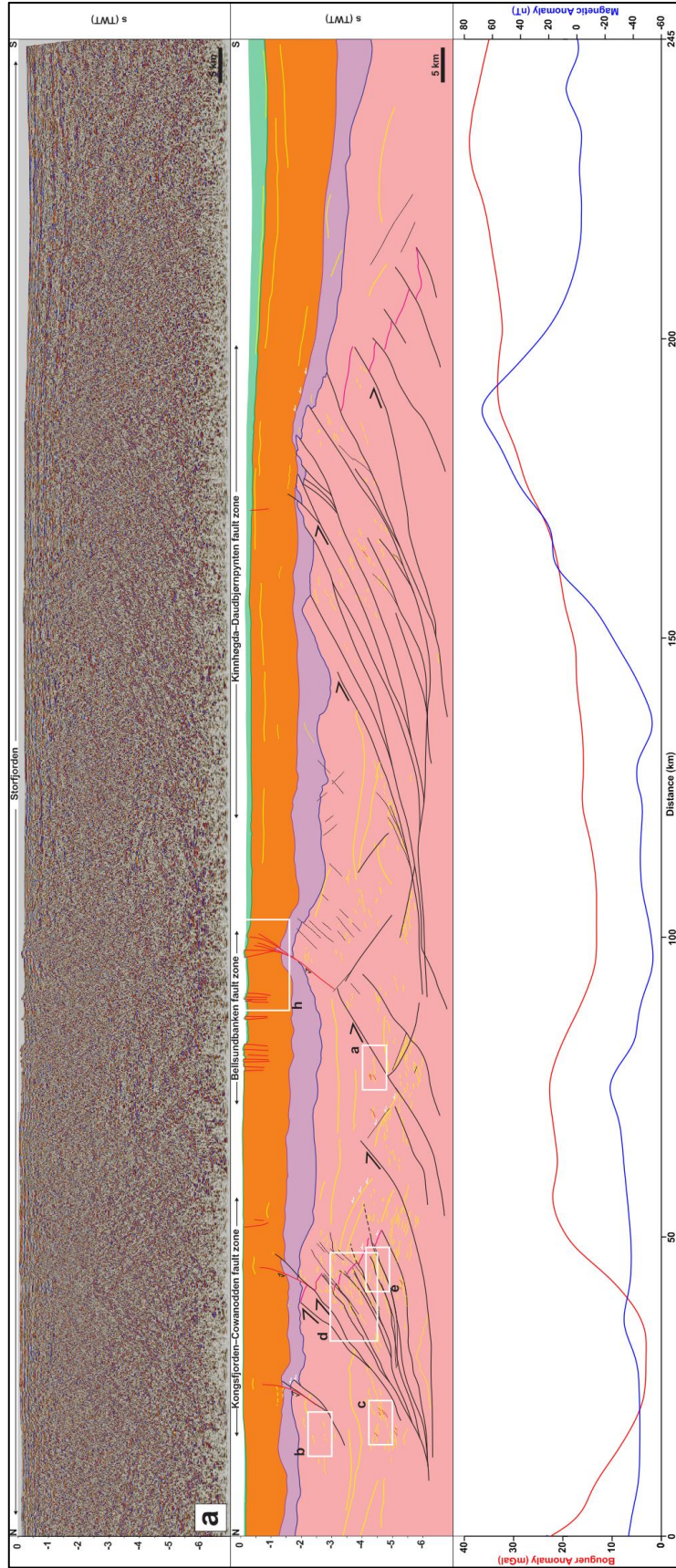


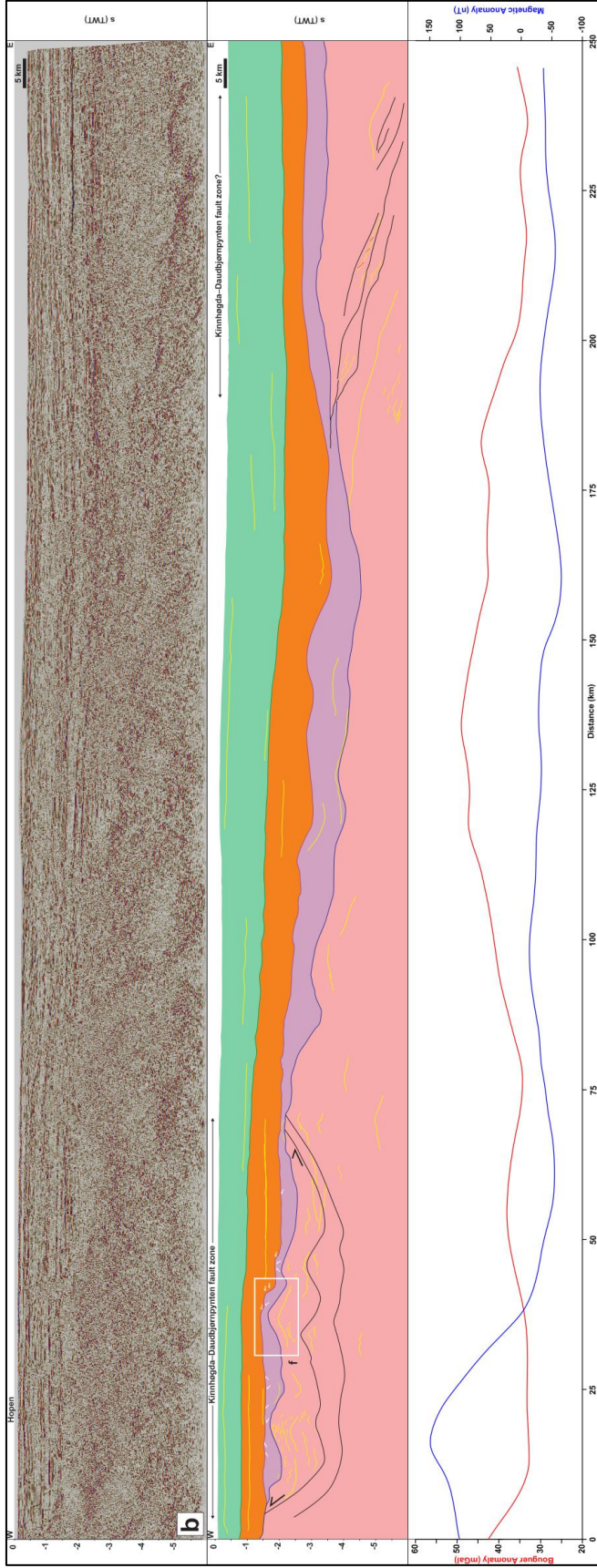
1581 **Figure 1: (a) Overview map showing the Timanian belt in Russia and Norway, and occurrences of Timanian fingerprints**
1582 **throughout the Arctic; (b) Regional map of Svalbard and the Barents Sea the main geological elements and the seismic**
1583 **database used in the present study. The location of (b) is shown as a white frame in (a); (c) Zoom in the northern Norwegian**
1584 **Barents Sea and Svalbard showing the main faults and basins in the study area, and the proposed Timanian structures. The**
1585 **location of (c) is shown as a black frame in (b). The location of the Raddedalen-1 well is from Smyrak-Sikora et al. (2020).**
1586 **Topography and bathymetry are from Jakobsson et al. (2012). Abbreviations: AA: Atomfjella Antiform; BaFZ: Baidaratsky**
1587 **fault zone; BeFZ: Bellsundbanken fault zone; BFZ: Billefjorden Fault Zone; Bi: Billefjorden; CTB: Central Tertiary Basin;**
1588 **HL: Heer Land; Hs: Hornsund; H2: Hopen-2; KCFZ: Kongsfjorden–Cowanodden fault zone; KDFZ: Kinnhøgda–**
1589 **Daudbjørnpynten fault zone; Kg: Kongsfjorden; LFZ: Lomfjorden Fault Zone; Nf: Nordmannsfonna; OgB: Olga Basin;**
1590 **OrB: Ora Basin; P1: Plurdalen-1; RA: Rijpdalen Anticline; R1: Raddedalen-1; Sa: Sassenfjorden; SB: Sørkapp Basin; Sf:**
1591 **Storfjorden; SH: Stappen High; SKFZ: Steiløya–Krylen fault zone; Te: Tempelfjorden; TKFZ: Trollfjorden–Komagelva**
1592 **Fault Zone; VKSZ: Vimsodden–Kosibapasset Shear Zone.**

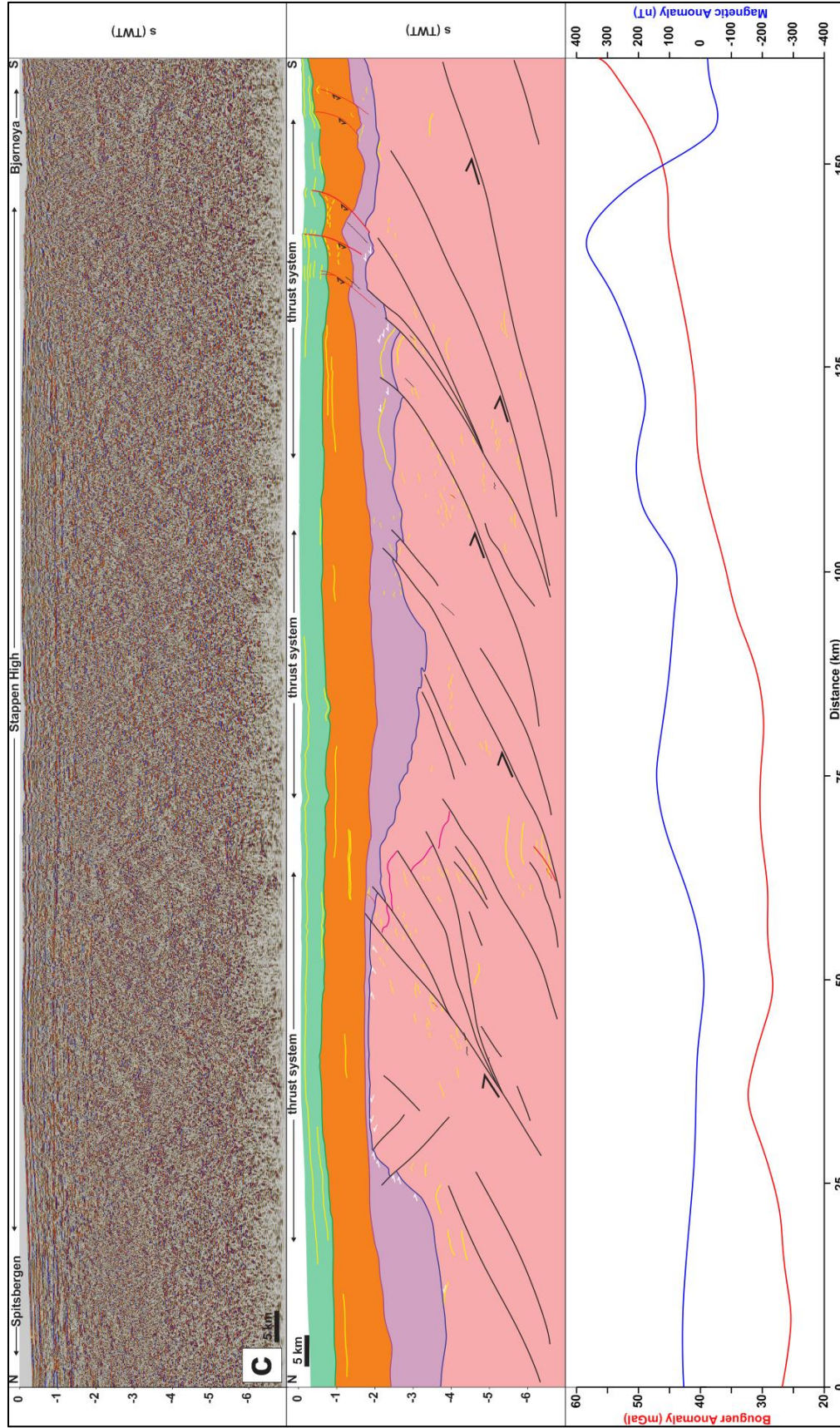


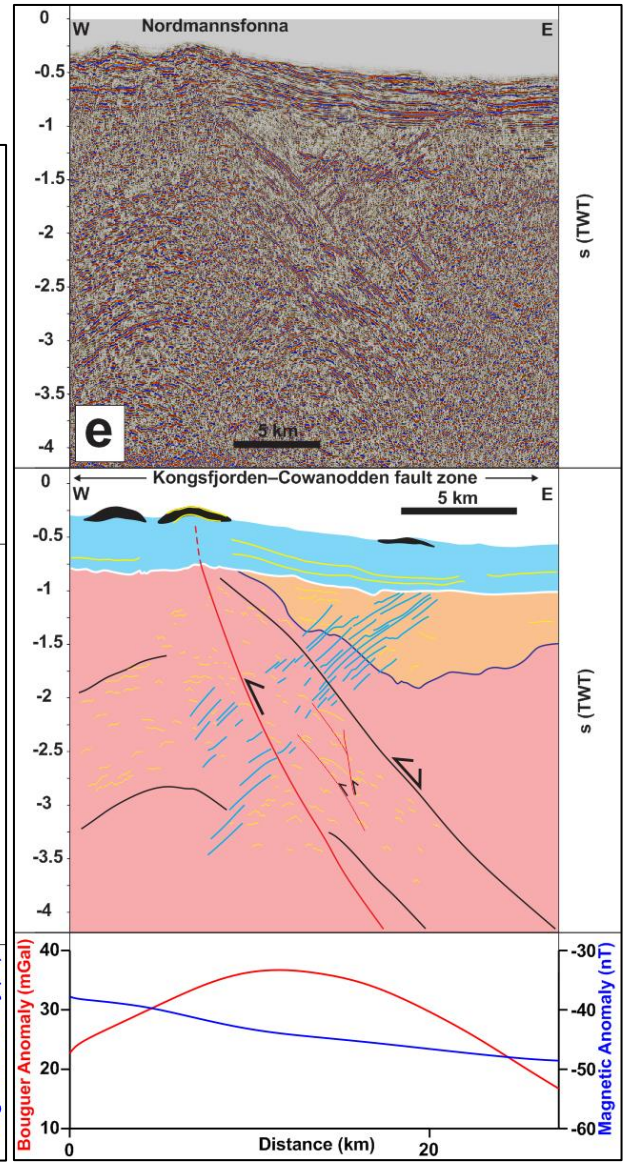
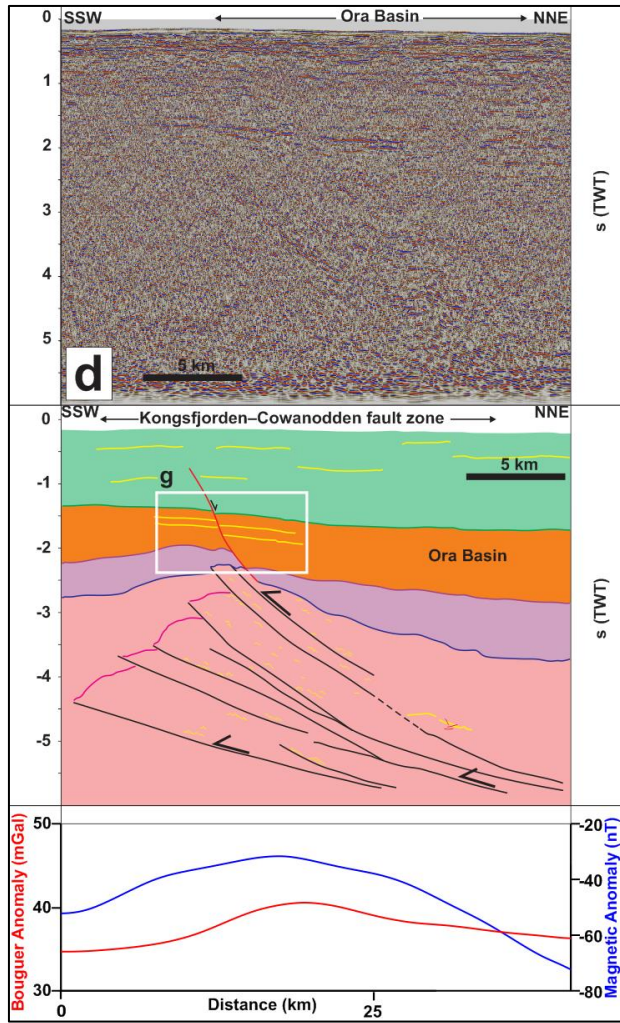
1593

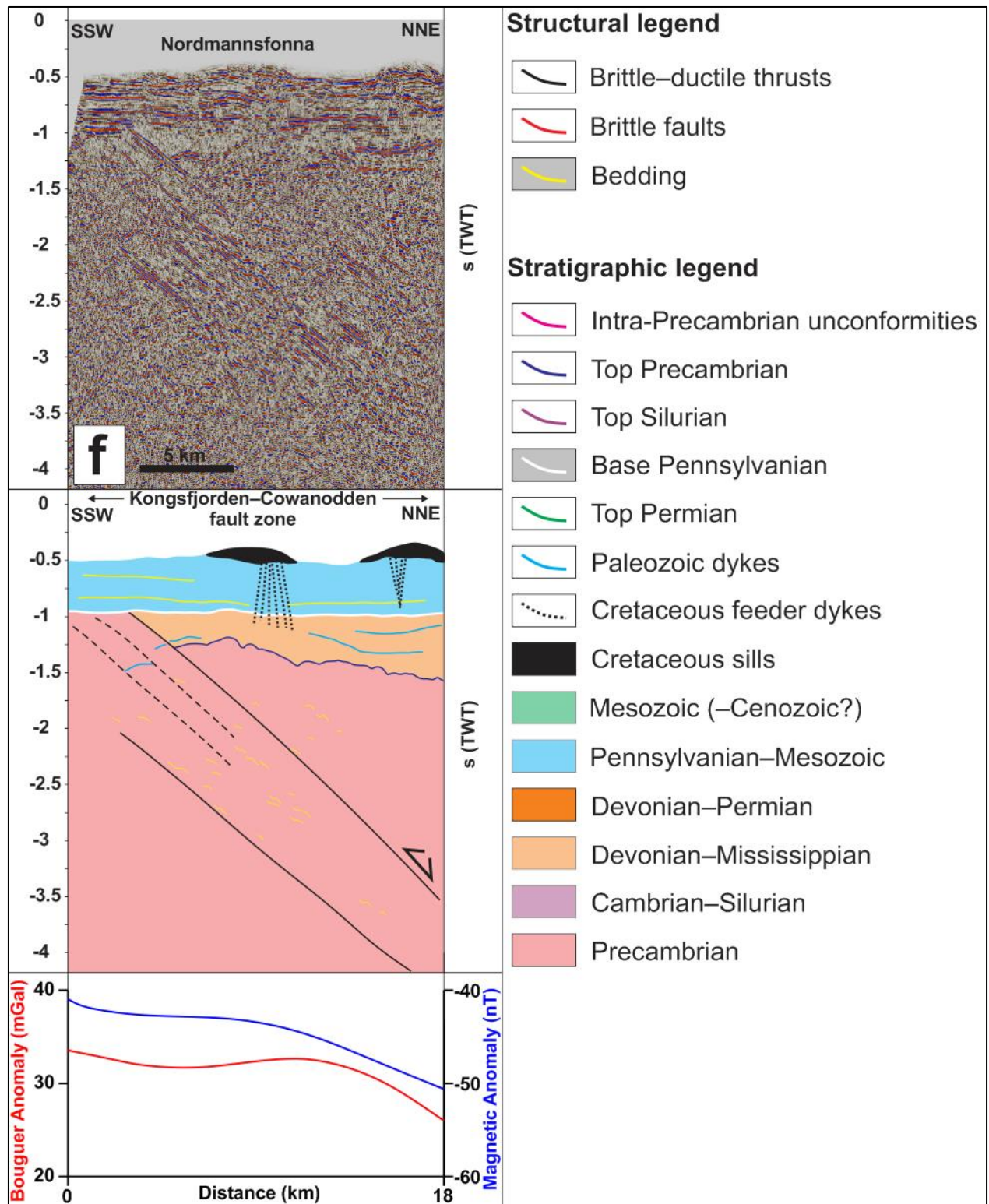
1594 **Figure 2: Paleogeographic reconstruction of the Svalbard Archipelago in the latest Neoproterozoic during the Timanian**
 1595 **Orogeny and in the early–mid Paleozoic during the Caledonian Orogeny according to previous models (e.g., Harland, 1969;**
 1596 **Labrousse et al., 2008).**









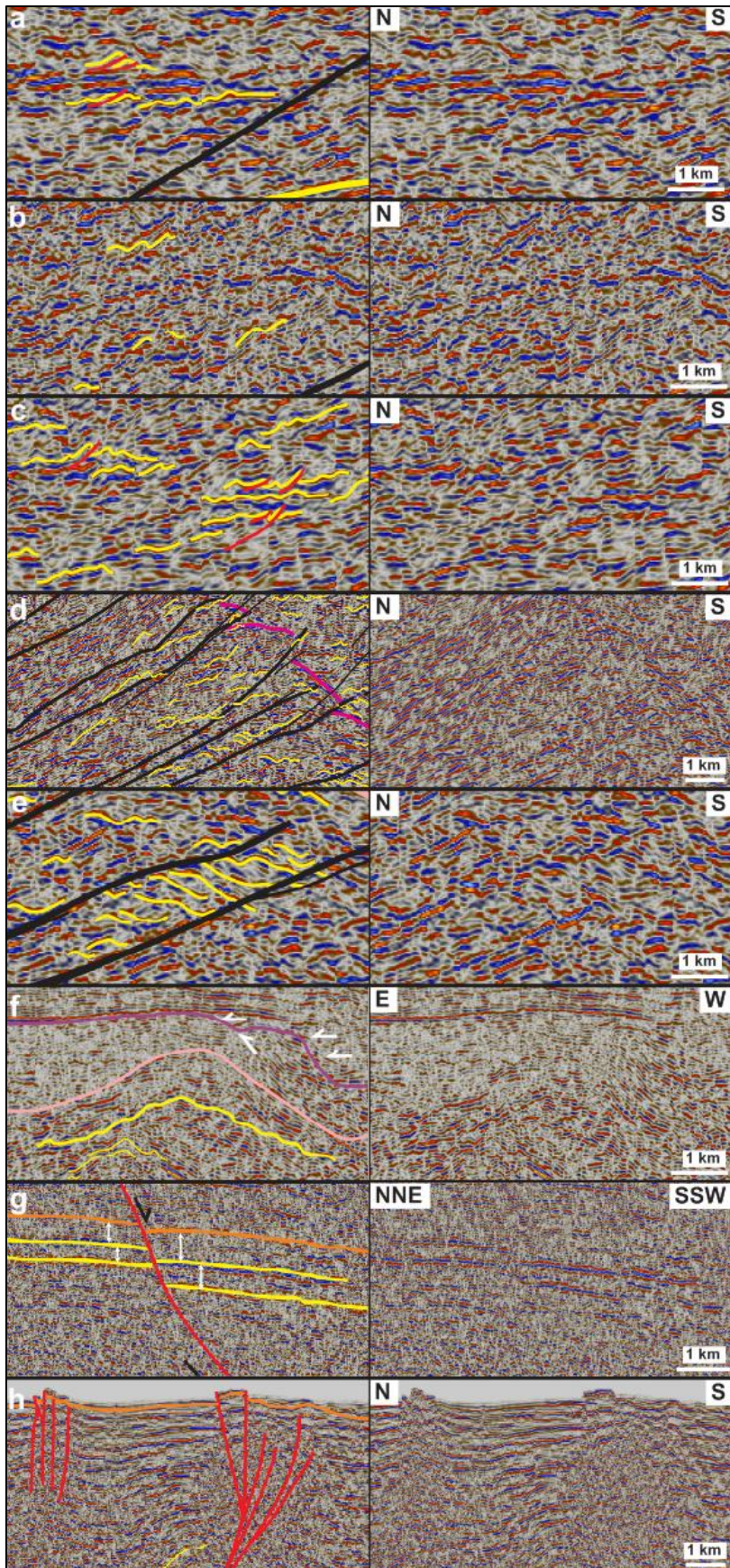


1601

1602 Figure 3: Interpreted seismic profiles and associated potential field data (a) in Storfjorden, (b) south of Hopen, (c) on the
 1603 Stappen High in the northwestern Norwegian Barents Sea between Spitsbergen and Bjørnøya, (d) on the southern flank of
 1604 the Ora Basin in the northeastern Norwegian Barents Sea, and (e and f) in Nordmannsfonna in eastern Spitsbergen. The
 1605 seismic profiles show top-SSW Timanian thrusts that were reactivated and overprinted during subsequent tectonic events
 1606 such as Caledonian contraction, Devonian-Carboniferous late-post Caledonian collapse and rifting, Eurekan contraction,
 1607 and present-day contraction. Profiles (e) and (f) also show Paleozoic and Cretaceous intrusions. The white frames show the

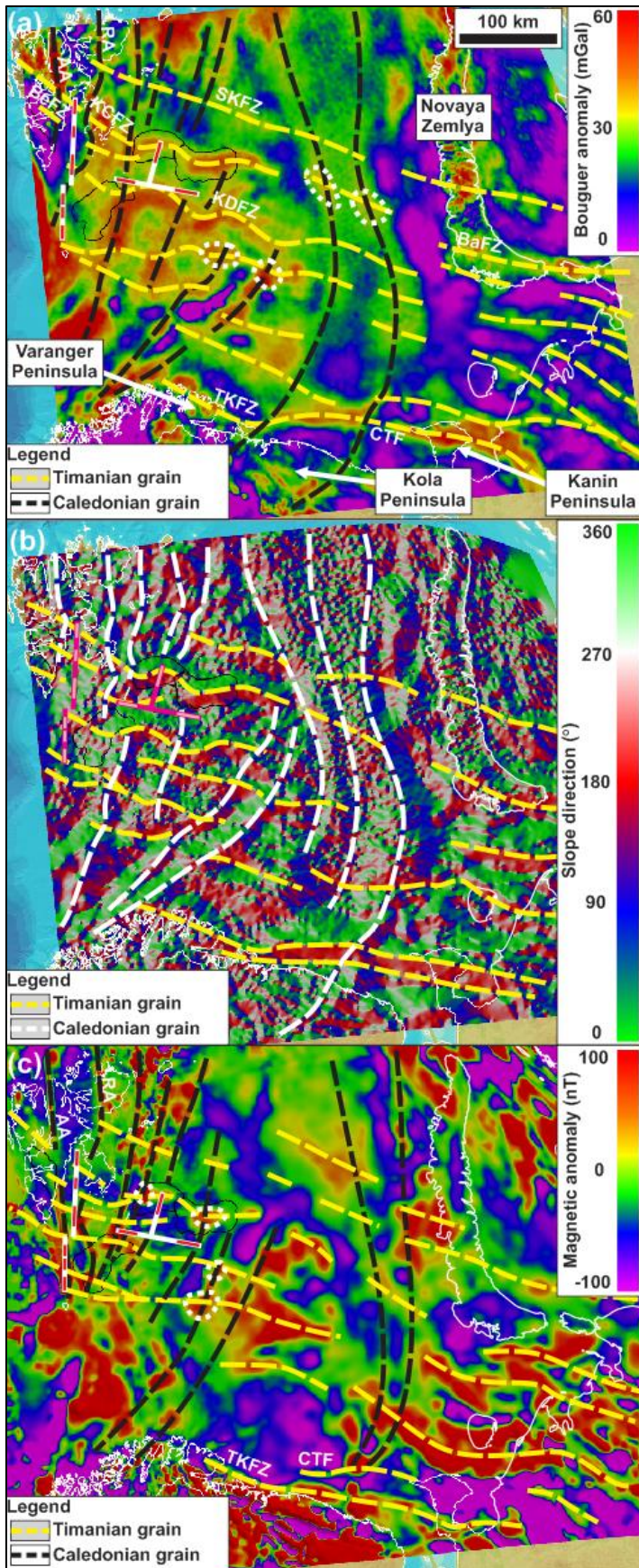
1608 location of zoomed-in portions of the profiles displayed in Figure 4. Potential field data below the seismic profiles include
1609 Bouguer anomaly (red lines) and magnetic anomaly (blue lines). The potential field data show consistently high gravimetric
1610 anomalies and partial correlation with high magnetism towards the footwall of each major thrust systems (i.e., towards
1611 thickened portions of the crust).

1612



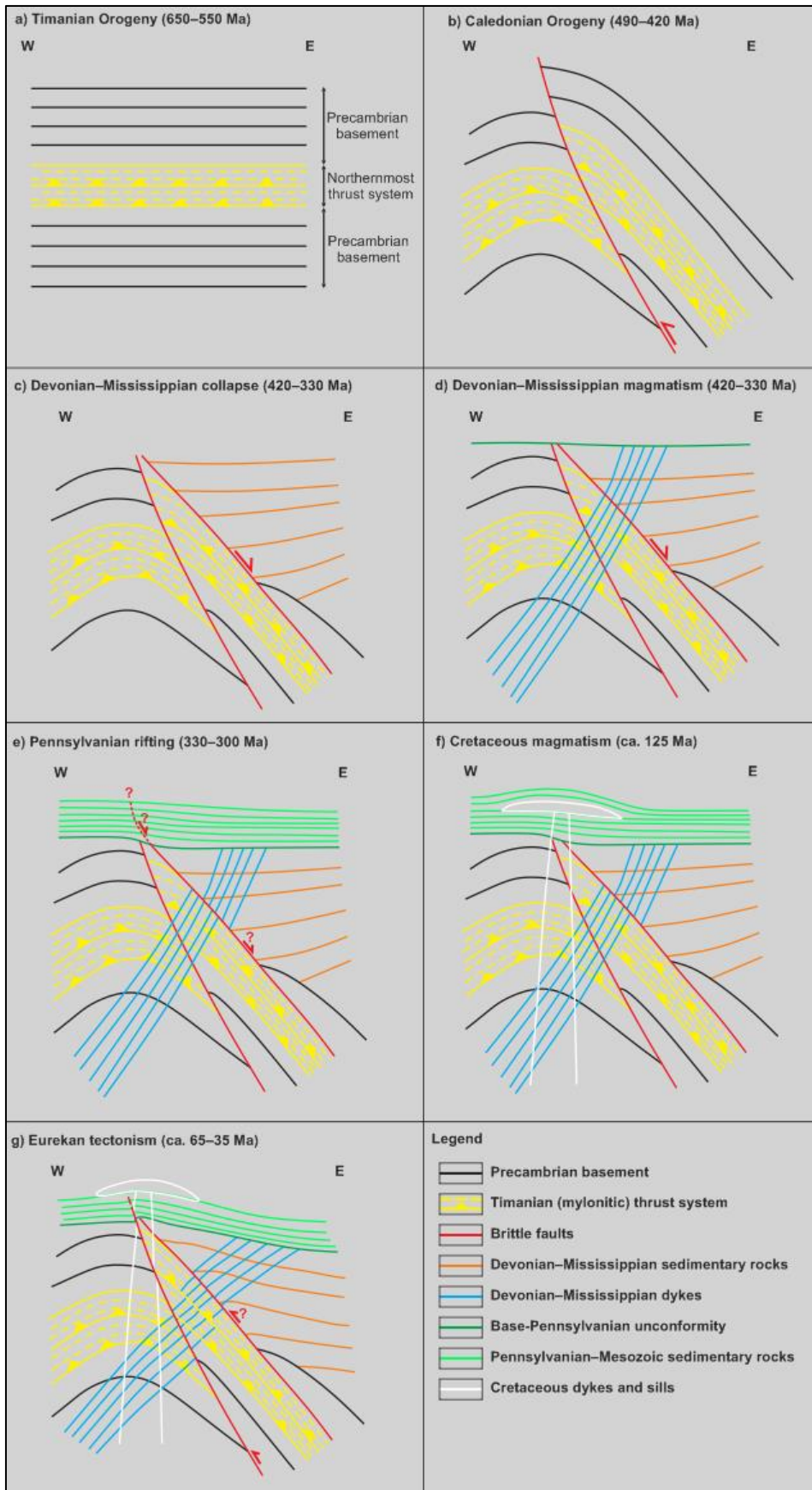
1614 **Figure 4: Zooms in seismic profiles shown in Figure 3 showing (a) upright fold structures, (b) SSW-verging folds and (c)**
1615 **top-SSW minor thrusts in Precambrian–lower Paleozoic (meta-) sedimentary basement rocks, (d) SSW-verging folds and**
1616 **NNE-dipping mylonitic shear zones within a major thrust that offsets major basement unconformities (fuchsia lines) top-**
1617 **SSW, (e) duplex structures within a major top-SSW thrust, (f) a N–S- to NNE–SSW-trending, 5–15 kilometers wide,**
1618 **symmetrical, upright macro-fold and associated, kilometer- to hundreds of meter-scale, parasitic macro- to meso-folds, (g)**
1619 **syn-tectonic thickening in Devonian–Carboniferous (–Permian?) sedimentary strata offset down-NNE by a normal fault**
1620 **that merges with a thick mylonitic shear zone at depth, and (h) recent–ongoing reverse offsets of the seafloor reflection by**
1621 **multiple, inverted, NNE-dipping normal faults in Storfjorden. See Figure 3 for location of each zoom and for legend.**

1622



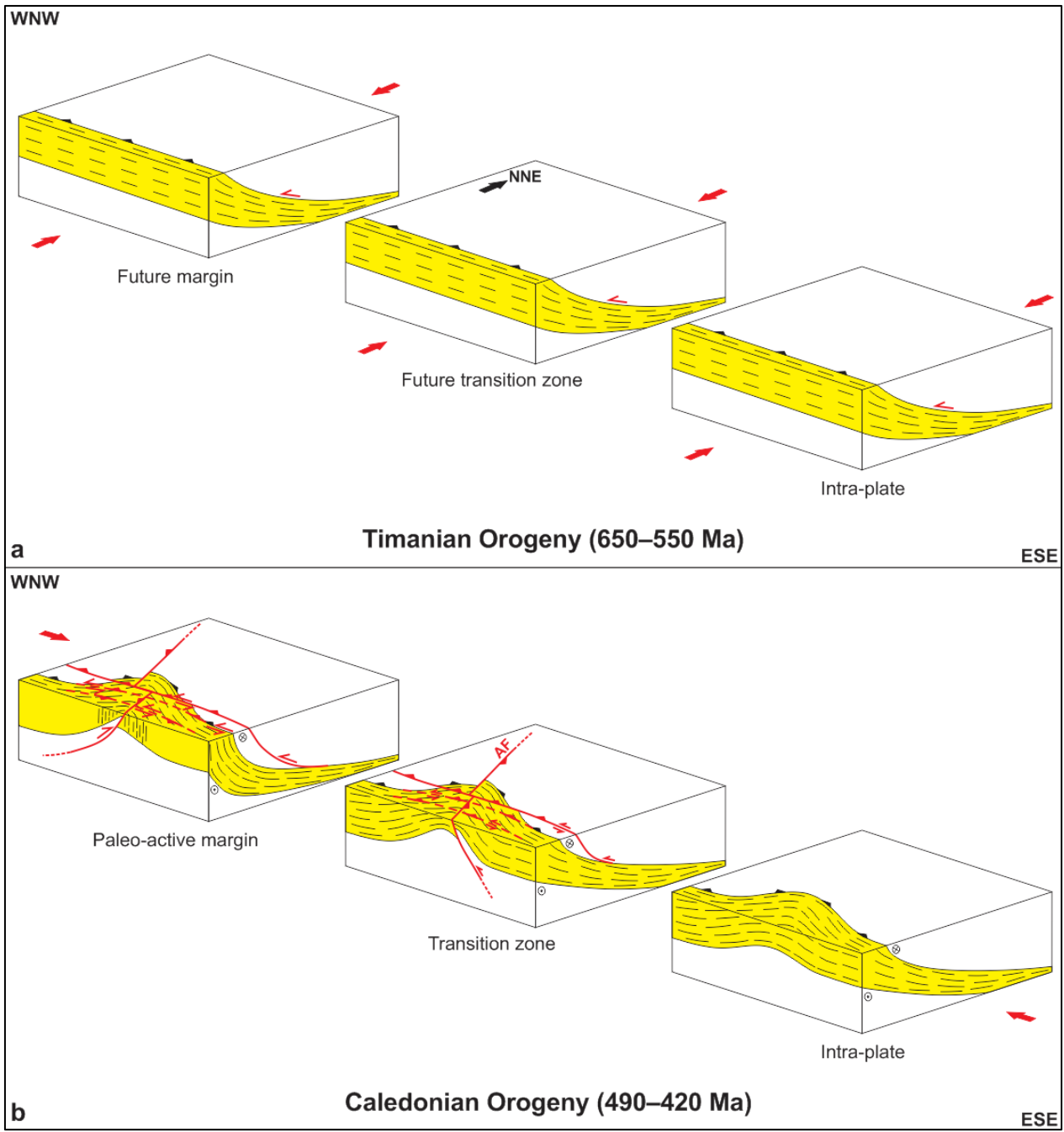
1624 **Figure 5: Gravimetric (a and b) and magnetic (c) anomaly maps over the Barents Sea and adjacent onshore areas in Russia**
1625 **(see location as a dashed white frame in Figure 1b), Norway and Svalbard showing E–W- to NW–SE-trending anomalies**
1626 **(dashed yellow lines) that correlate with the proposed NNE-dipping Timanian thrust systems in Svalbard and the northern**
1627 **Norwegian Barents Sea. Note the high obliquity of E–W- to NW–SE-trending Timanian grain with NE–SW- to N–S-trending**
1628 **Caledonian grain (dashed black/white lines). Note that dashed lines in (a) and (c) denote high gravimetric and magnetic**
1629 **anomalies. Also notice the oval-shaped high gravimetric and magnetic anomalies (dotted white lines) at the intersection of**
1630 **WNW–ESE- and N–S- to NNE–SSW-trending anomalies in (a) and (c) resulting from the interaction of the two (Timanian**
1631 **and Caledonian) thrust and fold trends. The location of seismic profiles presented in Figure 3a–d are shown as thick white**
1632 **lines in (a) and (c) and as fuchsia lines in (b). Within these thick white and fuchsia lines, the location and extent of thrust**
1633 **systems evidenced on seismic data (Figure 3) is shown in white in (a) and (c) and in pink in (b). For the E–W-trending seismic**
1634 **profile shown in Figure 3b, this implies that the red and pink lines represent N–S-trending synclines. Abbreviations: AA:**
1635 **Atomfjella Antiform; BaFZ: Baidaratsky fault zone; BeFZ: Bellsundbanken fault zone; CTF: Central Timan Fault; KCFZ:**
1636 **Kongsfjorden–Cowanodden fault zone; KDFZ: Kinnhøgda–Daudbjørnpynten fault zone; RA: Rijpdalen Anticline; SKFZ:**
1637 **Steiløya–Krylen fault zone; TKFZ: Trollfjorden–Komagelva Fault Zone.**

1638

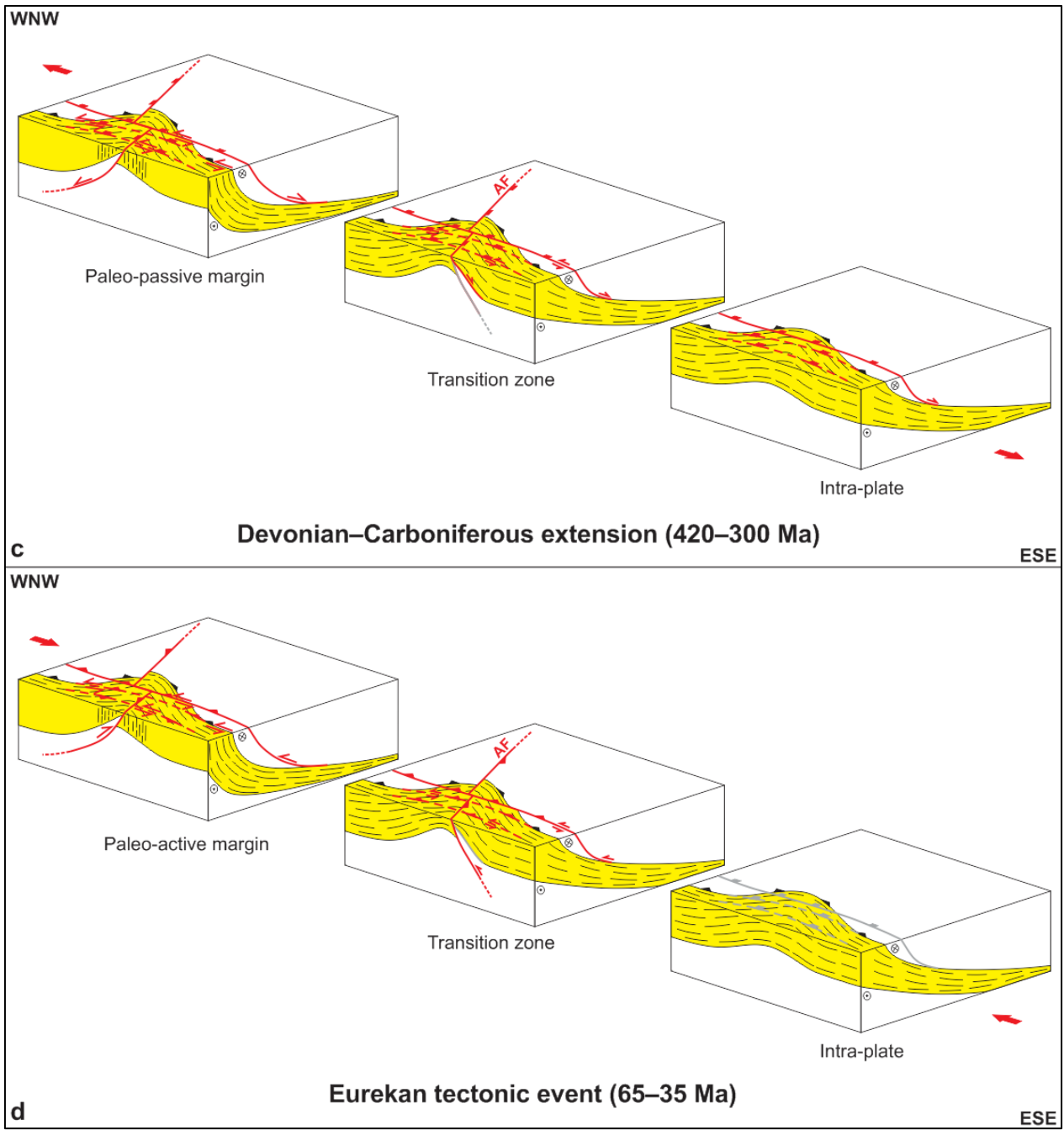


1640 **Figure 6: Sketches showing a possible reconstruction of the tectonic history of the E–W seismic profile in Nordmannsonna**
1641 **shown in Figure 3e. (a) Formation of a NNE-dipping, mylonitic thrust system (Kongsfjorden–Cowanodden fault zone)**
1642 **within Precambrian basement rocks during the Timanian Orogeny in the latest Neoproterozoic. The NNE-dipping**
1643 **Kongsfjorden–Cowanodden fault zone appears near horizontal on the E–W transect; (b) Top-west thrusting along the east-**
1644 **dipping Agardhbukta Fault and folding of the Kongsfjorden–Cowanodden fault zone into a broad, moderately NNE-**
1645 **plunging anticline during the Caledonian Orogeny; (c) Inversion of the Kongsfjorden–Cowanodden fault zone along the**
1646 **eastern flank of the Caledonian anticline and deposition of thickened, gently west-dipping, syn-tectonic, Devonian (–**
1647 **Mississippian?) sedimentary strata during post-Caledonian collapse-related extension; (d) Intrusion of Precambrian**
1648 **basement and Devonian (–Mississippian?) sedimentary rocks by steeply west-dipping dykes in the Devonian–Mississippian;**
1649 **(e) Regional erosion in the mid-Carboniferous (latest Mississippian) and deposition of Pennsylvanian sedimentary strata,**
1650 **possibly along a high-angle brittle splay of the inverted portion of the Kongsfjorden–Cowanodden fault zone during rift-**
1651 **related extension; (f) Deposition of Mesozoic sedimentary strata and intrusion of Cretaceous dolerite dykes and sills; (g)**
1652 **Erosion of Pennsylvanian–Mesozoic strata and reactivation of the Kongsfjorden–Cowanodden fault zone and Agardhbukta**
1653 **Fault with minor reverse movements in the early Cenozoic during the Eurekan tectonic event as shown by mild folding and**
1654 **offset of overlying post-Caledonian sedimentary strata, dykes and Base-Pennsylvanian unconformity. Also note the back-**
1655 **tilting (i.e., clockwise rotation) of Devonian–Mississippian dykes in the hanging wall of the Agardhbukta Fault and of the**
1656 **Kongsfjorden–Cowanodden fault zone.**

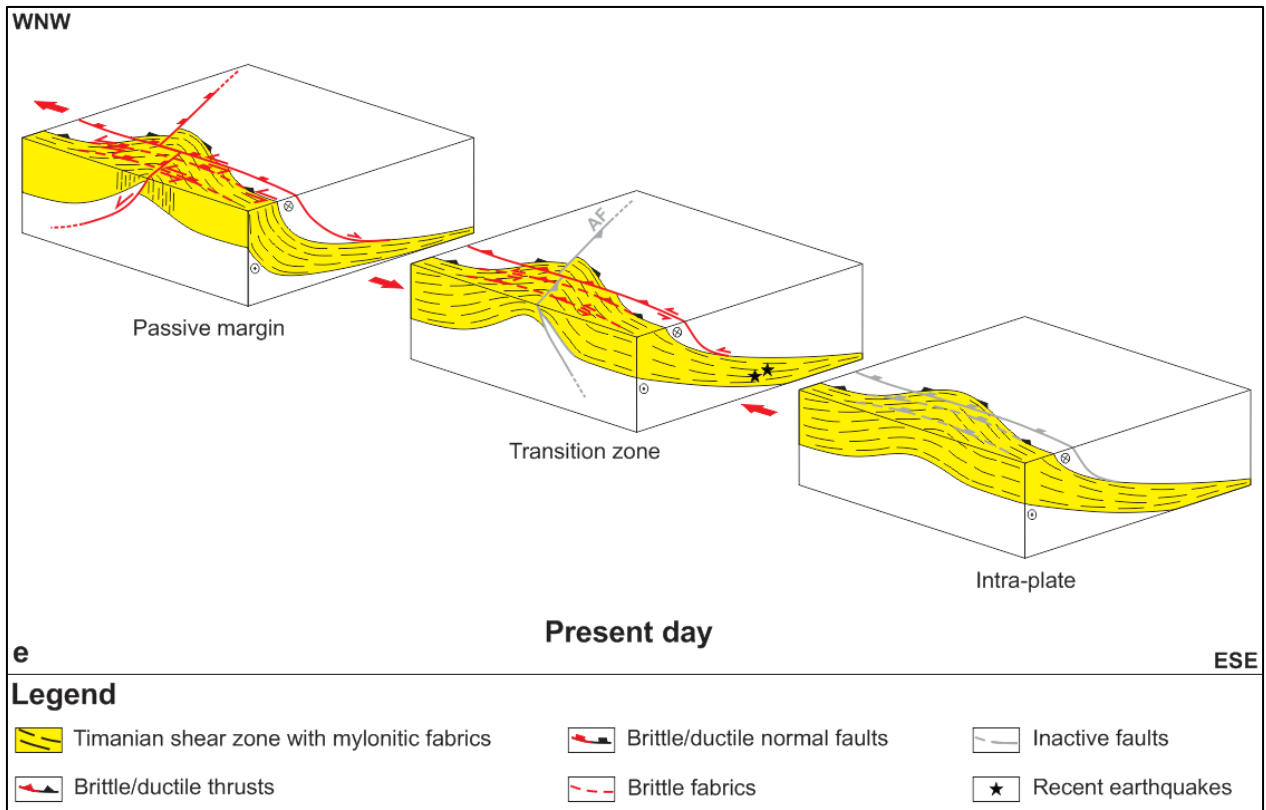
1657



1658

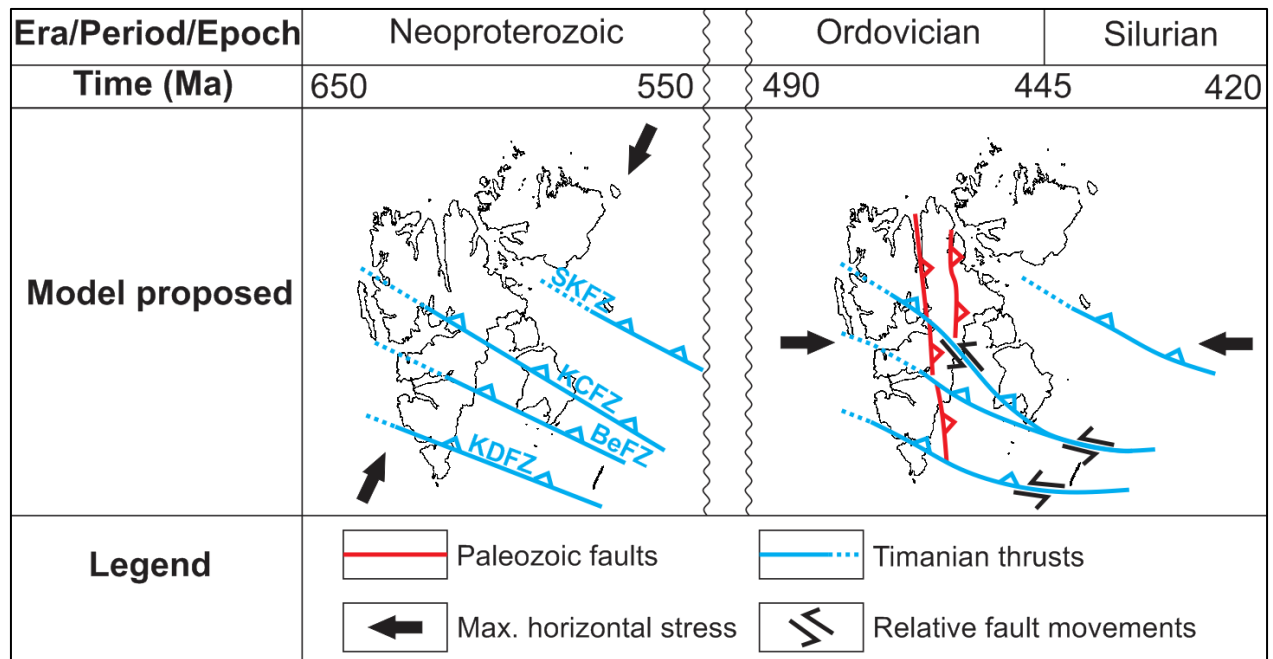


1659



1660
 1661 **Figure 7: Tectonic evolution of Timanian thrust systems in eastern and southern Spitsbergen, Storfjorden and the northern**
 1662 **Norwegian Barents Sea including (a) top-SSW thrusting during the Timanian Orogeny, (b) reactivation as oblique-slip**
 1663 **sinistral-reverse thrusts and offset by N–S-striking brittle thrust overprints (e.g., Agardhbukta Fault – AF) under E–W**
 1664 **contraction during the Caledonian Orogeny, (c) reactivation as low-angle, brittle–ductile, normal–sinistral extensional**
 1665 **detachments and overprinting by high-angle normal–sinistral brittle faults during Devonian–Carboniferous, late–post-**
 1666 **Caledonian extensional collapse and rifting, (d) reactivation as brittle–ductile sinistral–reverse thrusts, overprinting by**
 1667 **high-angle sinistral–reverse brittle thrusts, and mild offset by reactivated N–S-striking thrusts (e.g., Agardhbukta Fault –**
 1668 **AF) during E–W Eureka contraction (note the absence of reactivation and overprinting away from the margin), and (e)**
 1669 **renewed, recent–ongoing, sinistral–reverse reactivation and overprinting possibly due to ongoing magma extrusion and**
 1670 **transform faulting (ridge-push?) in the Fram Strait, i.e., normal-sinistral along the Fram Strait passive margin and reverse-**
 1671 **sinistral in the transition zone (e.g., Storfjorden and eastern Spitsbergen). Notice the relatively higher deformation intensity**
 1672 **of Timanian thrusts at (paleo) active and passive margins including sub-vertical geometry prone to accommodate lateral**
 1673 **movement (e.g., Vimsodden–Kosibapasset Shear Zone in southern Spitsbergen), and milder reactivation–overprinting**
 1674 **away from the margin where Timanian thrusts retained their low-angle geometry (e.g., eastern Spitsbergen, Storfjorden, and**
 1675 **central Barents Sea). Folding of Timanian thrusts is also more gentle away from the margin (e.g., central Barents Sea, and**
 1676 **Olga and Ora basins).**

1677



1678

1679

1680

Figure 8: Paleogeographic reconstruction of the Svalbard Archipelago in the latest Neoproterozoic during the Timanian Orogeny and in the early–mid Paleozoic during the Caledonian Orogeny according to the present study.